2017

Hyporheic Flow Possibilities within Lamprey (Petromyzon marinus) Redds on the Blackledge River in Marlborough Connecticut

Samuel Fixler
Connecticut College, sfixler@conncoll.edu

Hyporheic Flow Processes within Lamprey (*Petromyzon marinus*) Redds on the Blackledge River, in Marlborough, Connecticut

Samuel Fixler

An Honors Thesis submitted in partial fulfillment
of the requirements for the degree of Bachelor of Arts
Environmental Studies
Connecticut College
May 2017

Supervised by:

Douglas M. Thompson, Ph.D.
Chair, Department of Physics, Astronomy, and Geophysics, Connecticut College

Beverly A. Chomiak, Ph.D.
Senior Lecturer in Geology and Senior Lecturer in Environmental Studies, Connecticut College

Table of Contents

Acknowledgements

I would like to express my gratitude to my advisor Doug Thompson for his encouragement and guidance throughout the process of this study. His assistance, patience, and knowledge were crucial in the development of this study. Doug's mentorship and passion for rivers has made a huge impact on the direction of my education. I would like to thank Beverly Chomiak for her critical analysis as a second reader and her ability to encourage my best work. I would also like to thank Kali Roberts for her assistance in data collection over the summer of 2016, and her continued support throughout this process. Thank you so much.

List of Figures

List of Tables

List of Equations

Fixler, Samuel A., Hyporheic Flow Processes within Lamprey (*Petromyzon marinus*) Redds on the Blackledge River, in Marlborough, Connecticut: unpublished honors thesis, Connecticut College, New London, Connecticut.

1. Abstract

The fluvial geomorphic process of hyporheic flow provides critical nutrients and dissolved oxygen to macroinvertebrates and eggs within riverbeds through hyporheic exchange. Hyporheic flow may operate at similar scales within sea lamprey (*Petromyzon marinus*) redds. Limited documentation exists on the hyporheic processes within lamprey redds. This study attempts to measure hyporheic flow using a saline injection syringe and salinity probe to record salinity-time curves. The method was applied to several redds on the Blackledge River, Marlborough, Connecticut. The second aspect of this study examined the hydraulic properties of lamprey redds within a controlled environment in a 0.5 m by 6 m flume at Connecticut College, New London, Connecticut. A 50% scale redd was constructed and velocity measurements were taken using an acoustic Doppler velocimeter at three different discharges. The salinity syringe provided moderate success in measuring the percent change of salinity and decay rate, with the strongest correlation at the beginning of the mound, but failed to provide accurate intergranular velocity measurements. The results of the flume study indicate strong areas of downwelling and upwelling at the pit and mound, respectively. Turbulent kinetic energy (TKE) is highest over the mound, indicating different pressures that may induce hyporheic flow through the redd mound. Velocity was the slowest downstream of the mound for all three discharges, and mean vertical velocity (Vz) values increased then decreased rapidly moving downstream over the mound. Although the hyporheic flow was not directly measured, the results reveal that lamprey redds

influence localized velocity patterns and create low pressures downstream of the mound, which should enhance hyporheic exchange.

Key terms: Hyporheic flow, hyporheic exchange, complexity, scalability, hydraulic conductivity, redd, supercritical flow.

2. Introduction

The hyporheic zone is an active region between the surface water of the main channel and groundwater. The hyporheic zone is present in all rivers, streams, and creeks and it provides vital habitat for macroinvertebrates and fish species that rely on the interstitial spacing between the sediment. The exchange between the hyporheic zone and surface water, nutrients, and organic matter respond to variations in discharge, bed topography, and porosity (Boutlon et al., 1998; Brunke and Gonser, 1997). The process of hyporheic flow provides the exchange of critical nutrients and dissolved oxygen (DO) to organisms within the bed. The goal of this thesis is to examine hyporheic flow at lamprey redds on the Blackledge River in central Connecticut. Redds are a nest of eggs created by spawning lamprey, and are used for reproduction and breeding. This will be achieved by surveying water velocities and topography within lamprey redds with the objective of learning the manner of hyporheic flow through lamprey redds. This study compares hyporheic processes using two different methods. The study involves a field portion complimented by a laboratory experiment. The field investigation involves obtaining velocity measurements within the hyporheic zone using a salinity injection syringe method. This method quantified hyporheic flow by measuring it directly. The laboratory experiment involved the creation of an artificial lamprey redd within a recirculating flume. This process measured hyporheic flow in a 0.5 m by 6.0 m flume at Connecticut College, New London, Connecticut indirectly by measuring velocities above the redd in the surface water to indicate areas of low and high pressures where upwelling and downwelling can be correlated to incidences of hyporheic flow.

The artificial redd experiment is hypothesized to create areas of upwelling and downwelling in the redd, at the pit and mound, respectively. It is expected that the velocity

patterns moving downstream will create an area of low pressure and a wake zone just downstream of the mound. The wake zone will force water upstream because of the low pressure zone and cause movement through the interstitial spacing in the mound. The resulting movement would signal the presence of hyporheic flow. The expected result of the salinity syringe experiment is that the readings will show a percent change in salinity over time, which will indicate a decay rate and give insight into the retention and function of hyporheic exchange within the redd. The field experiment is predicted to suggest higher levels of salinity readings close to the pit and mound injection sites, which would imply the presence of flow moving through the redd.

2.1. The Hyporheic Zone

Downwelling and upwelling from the hyporheic zone play important roles in the function of a riverine ecosystem. The downwelling provides dissolved oxygen and organic matter to organisms in the hyporheic zone, while upwelling delivers stream organisms with nutrients. This process is called hyporheic exchange and is represented by the water volume per time (m^3/s) that enters and subsequently exits the porous area at the top of the hyporheic zone (Trauth et al., 2013). Hyporheic exchange is the flow between groundwater and surface flow, hyporheic flow and surface water, or the flow between groundwater and the hyporheic zone The hyporheic

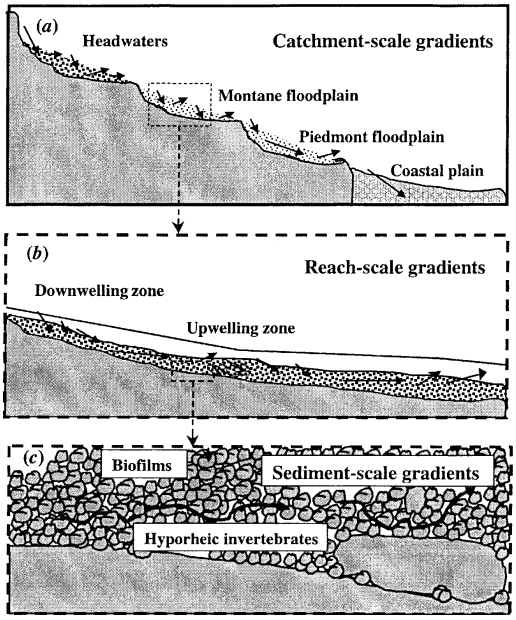

Figure 2.1. Illustrates the scale at which the hyporheic zone operates, and the various progressions within (Boutlon et al., 1998).

zone and exchange that occurs at deep pools and following shallow riffles at the pool-riffle stage is especially important for fish species like lamprey and salmon that spawn in the interstitial spaces in riffle reaches. The hyporheic zone plays an important function both geomorphically and ecologically in pool-riffle systems. Unfortunately, management strategies typically overlook its importance in favor of fish-level restoration (Boulton et al., 1998; Findlay, 1995).

The hyporheic zone hosts different forms of lateral, vertical, and longitudinal movement of water through the bed of the channel. The type of movement depends on the morphology of the channel. The exchange processes of the hyporheic zone also contain different scales that provide different functions like exchange with groundwater or channel flow (Figure 2.1, 2.2, and Figure 2.3).

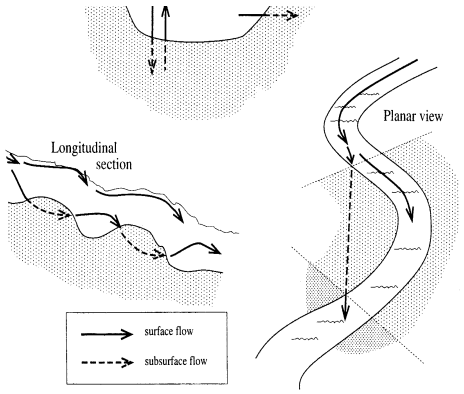

Fig. 1. Diagram showing vertical and lateral exchanges of water between the open channel and surrounding saturated sedimen
he hyporheic zone (shaded region). The pathways and geomorphic features are common but not the only possible features abl
nduce hyporheic exchange.

Figure 2.2. Shows a simplified view of hyporheic exchange in relation to surface flow and subsurface flow (Findlay, 1995).

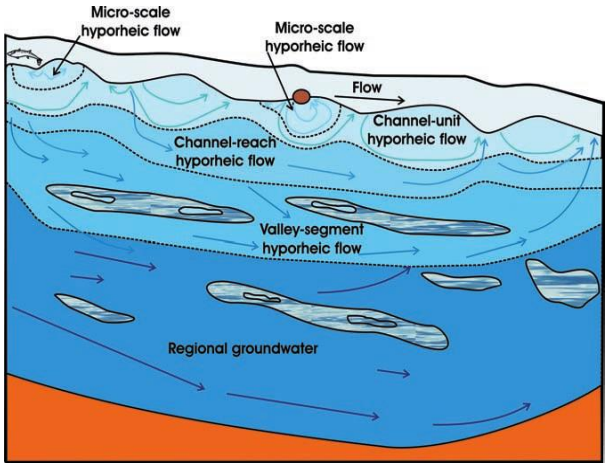

Figure 2.3. The different longitudinal profile scales of hyporheic exchange; boundaries in scales are indicated by dashed lines. Three-dimensional hyporheic flow occurs in and out of the diagram. (Buffington and Tonina, 2009).

The aim of this study is to provide new insight into the processes and functions of hyporheic flow within lamprey redds. An additional goal of this study is to quantify the importance of hyporheic exchange and its biological functions, hopefully providing insight into the reason for lamprey redd creation.

3. Background

The hyporheic zone can be altered by many different factors. Different variations in flow produced by hydraulic jumps, which is a phenomenon when water travelling at a supercritical velocity suddenly slows down to subcritical conditions and causes an abrupt rise in the surface height of the water. These jumps typically precede a riffle zone and can change the profile and characteristics of the hyporheic zone (Trauth et al., 2013). The trough of a standing wave or jump corresponds with the highest streambed pressures, which can result in changes in the 3-D hyporheic flow field (Trauth et al., 2013). This interpretation of the hyporheic zone has important implications for the hyporheic zone and its relationship to organisms that rely on it.

Conditions that limit exchange flow result in groundwater discharge that is 5-20 times greater than at the sides of a stream (Storey et al., 2003). This suggests that the impact to hyporheic exchange is most noticed at the sides of the system rather than the middle. If a stream has been modified for erosion control at the banks, then the potential for hyporheic exchange with the adjacent groundwater might be limited because exchange flows tend to be greater at the sides than at the center of the channel. In some cases, groundwater discharge inhibits lateral and vertical flow in the hyporheic zone at the sides of the channel, but vertical exchange still occurs underneath the center of the channel (Storey et al., 2003). In settings that permit exchange flow, outwelling and downwelling in the hyporheic zone at the sides of the channel is up to twice that of the center of the channel (Storey et al., 2003). These findings have important implications for the hyporheic zone because lack of lateral movement and downwelling prevents important oxygen and nutrient exchange necessary for microorganism and macroorganisms.

Temperate streams can have hydraulic conductivity that can vary up to 40% with seasonal variations in water temperature (Storey et al., 2003). These occurrences are a result of

the relationship of density and temperature. Hydraulic gradients between upstream and downstream riffles can decline by half in the winter, and groundwater discharge can increase by a factor of two or more (Storey et al., 2003). These factors can result in a ten to thirtyfold reduction in hyporheic exchange in low-gradient, temperate streams during winter (Storey et al., 2003). The reduction of hyporheic exchange in low-gradient streams, like a pool-riffle system, can critically reduce the healthy functioning of the ecosystem. The reduction can also limit the developmental ability of gravel-spawning fish, and the abundance of macroorganisms and microorganisms. These findings coupled with a modified stream bed can severely diminish the rate of hyporheic exchange, especially in a pool-riffle system. In a pool-riffle system that has a healthy hyporheic zone, the flow rates can greatly affect the efficiency of the hyporheic zone ability to support a healthy trophic network or multiple levels of organisms in the food chain. The morphological function of an unhealthy hyporheic zone is poorly understood and so is the specific morphological functions of the hyporheic zone itself.

Historically, measuring hyporheic-flow conditions involved using tracer fluids, like dyes and saline solutions, to characterize hyporheic exchange. However, these sensitivity tracer methods at higher base flows causes bias towards only fast and shallow hyporheic exchange (Harvey et al., 1996). The current method makes use of tracer models that consider multiple rate constants that measure two different rates of both faster exchange with streambed gravel and slower exchange with deeper alluvium (Harvey et al., 1996; Castro and Hornberger, 1991). These methods help better predict the function of hyporheic exchange in pool-riffle systems. There are also computational models that predict different simulated flow patterns with variations in channel width, sediment size, stream gradient and other variables. Models and tracer particle methods applied to specific channel morphologies will contribute to a better

understanding of the geomorphological function and resulting ecological function of hyporheic exchange. The next step for methods might be also applying hydrological and biogeochemical models that help explain stream ecosystem behavior (Findlay, 1995). Combining geomorphological simulations to these models might also add another level of understanding for the geomorphological and ecosystem-level importance of hyporheic exchange.

The study of the hyporheic zone and the exchange processes it exhibits are important for understanding the ecological roles of the organisms within it, and how these organisms react to changes in the hyporheic zone. For example, if lateral hyporheic exchange has higher seasonal variability than vertical exchange, then the biological community lateral to the stream channel will experience higher levels of physiochemical variance than the community beneath (Storey et al., 2003). In these conditions microorganisms and macroorganisms with flexible metabolisms might be favored in more variable areas of the hyporheic zone (Storey et al., 2003). If the sides of the channel experience stronger downwelling and upwelling than the center, then a spatial and temporal pattern in the biogeochemical processes may be created because of responses to the replenishment of resources (Storey et al., 2003). These conditions might be especially apparent in a pool-riffle channel.

In low channel gradient pool-riffle system there is much more spatial variation in sediment size, and as a result hyporheic exchange is expected to be more complex, slower and deeper (Buffington and Tonina, 2009; Harvey and Bencala, 1993). Hyporheic exchange in pool-riffle channels is much more complex because of the unconfined valleys in which they generally occur. These channel types generally have much more lateral hyporheic exchange (Buffington and Tonina, 2009). Meander bends, divided channels, floodplain bodies, and paleochannels all play important roles in promoting hyporheic exchange, which is why the complex network in a

pool-riffle system creates more chances for hyporheic exchange (Buffington and Tonina, 2009). The pool-riffle system also has widely varying sediment sizes which create opportunities of rapid rates of exchange, but the alluvial fines also promote deeper and longer flow paths for hyporheic exchange, but less hydraulic conductivity near the surface (Buffington and Tonina, 2009). Because of the complex hyporheic patterns a pool-riffle system contains, there is generally a longer residence time compared to steeper more confined channels (Buffington and Tonina, 2009; Kasahara and Wondzell, 2003).

In comparison, in higher-gradient channels, like cascades and step-pools, one would expect a faster and shallower rate of exchange (Buffington and Tonina, 2009). This factor corresponds with a pool-riffle system generally having higher abundance and diversity of aquatic and riparian organisms (Buffington and Tonina, 2009), illustrating that hyporheic flow most likely plays a much more important role in terms of productive habitats in lower gradient systems. Pool-riffle systems most likely have the best range of scale of hyporheic exchange, especially those that occur in broad alluvial valleys (Buffington and Tonina, 2009).

The subsurface flow in pool-riffle system has several distinctive characteristics in flow, like multiple scales of turbulence and near-bed pressure fluctuations, but the hyporheic exchange from this pool-riffle system is most likely minor because a layer of coarser sediment is usually found above a layer of finer sand, which most likely would dampen the turbulence induced hyporheic flow (Buffington and Tonina, 2009). Thus, hyporheic exchange will vary with the spatial variation in sediment type and size (Buffington and Tonina, 2009). Significant sediment transport generally only occurs at bankfull flows on pool-riffle channels, thus, locational change of hyporheic exchange is limited to these events (Buffington and Tonina, 2009). Therefore, the distribution of hyporheic zones is much more steady compared to systems with more varied

discharges. The greater percentage of the hyporheic exchange allows for the higher relative abundance of hyporheic organisms in a pool-riffle system compared to higher-gradient channels.

Anthropogenic effects can have significant impacts on channel morphology at multiple scales. The influence of anthropogenic modifications can also effect the hyporheic zone at multiple scales. The impact of anthropogenic effects on the hyporheic zone, however, has not been studied as thoroughly as the effects on bed features.

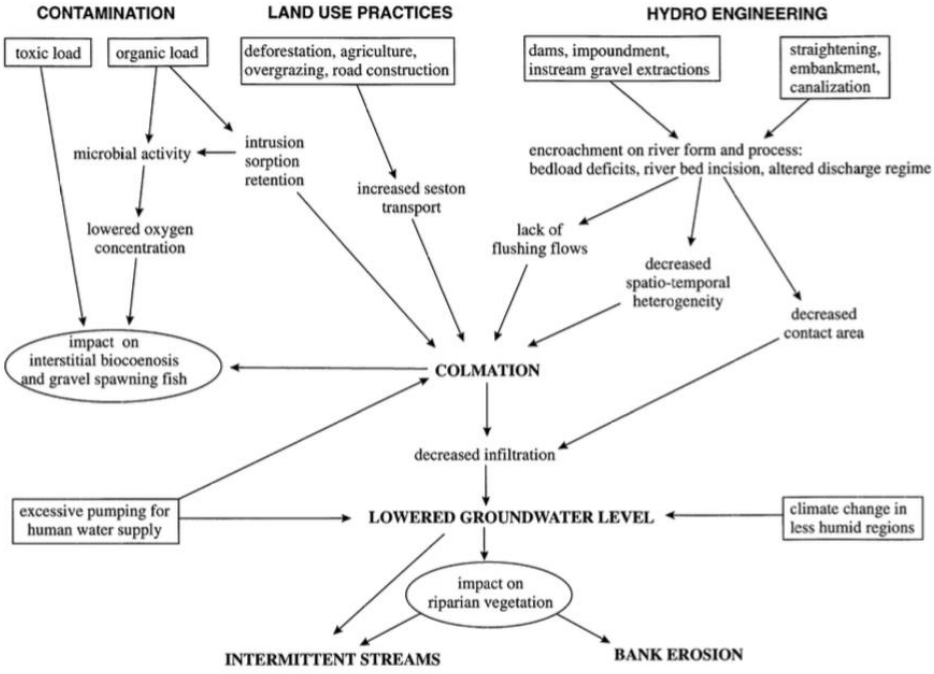

Figure 3.1. Anthropogenic impacts that encourage colmation, which is the clogging of sediments in top layer of the stream bed (Brunke, 1999; Brunke and Gonser, 1997; Veličković, 2005).

When a river system is modified by anthropogenic forces that result in increased or decreased discharge, the hyporheic zone can be damaged. In a low-gradient stream system, hyporheic exchange is only possible with highly permeable materials surrounding the stream channel (Storey et al., 2003). Streambed morphology at pool-riffle systems is affected by bank erosion controls and large wood (LW). Sediment dynamics are limited by LW and erosion controls, subsequently resulting in a small ratio of pool-riffle wavelength to stream width

(Montgomery et al., 1995; Trauth et al., 2013). These factors might limit the standing pressure at the hydraulic jump, which would result in a smoother hydraulic zone pool-riffle transition with fewer hydraulic jumps (Trauth et al., 2013). Increased sediment loads and the effects of pollution can drastically effect the hyporheic zone and its inhabitants because of longer residence times found in the hyporheic zone. Natural variations in the hyporheic zone are important for promoting different levels upwelling and downwelling (Cardenas et al., 2004). However, it is important to note that complexity in river morphology is important for fulfilling different ecological niches. The different types of river morphology, whether a pool-riffle system or a meandering system, satisfy the needs of different organisms. The change in a river system's morphology is what makes it healthy.

The rate of modification, whether it includes dams, erosion control, or poor habitat structures, can cause drastic changes in the rate of sediment deposition in pool-riffle systems (Brandt, 2000). Channel morphology and its relationship to the hyporheic zone can certainly have negative effects throughout the whole system. It is unclear how important the hyporheic zone and the exchange processes that take place are to the health and the ecological function of the stream, but a lot of organisms do rely on these processes. Without the nutrient and dissolved oxygen (DO) exchange that takes place in the hyporheic zone, it can be assumed that there would be an upscaling-trophic-cascade effect on species that rely on these processes (Brunke and Gonser, 1997). The failure of organisms at the bottom of the trophic network would cause a collapse of the network to the top. Because the hyporheic zone is relatively poorly understood, it is difficult to assess the impacts of anthropogenic modification beyond general assumptions, like the relationship that bank erosion, hydro-engineering, contamination, and land-use practices have on the hyporheic zone's effectiveness (Figure 3.1). Most of the impacts would be a result of

increased sediment transport, which would have an effect on the interstitial spacing between gravel particles. The most obvious result of this would be on gravel-spawning fish and macroinvertebrates.

In pool-riffle channels, the anthropogenic impacts on the hyporheic zone are likely to be much greater than in a steeper system. Thus, the impact on gravel-spawning fish species is likely to be much greater at this channel type as well. The impact of chemical pollution also has a gradual and prolonged effect on the hyporheic zone because of the long residence times it exhibits at the pool-riffle level. Long pollution decay time, which is the rate pollution remains in a system, would have a negative impact on organisms that rely on the hyporheic zone. The impact of eutrophication events is likely to increase as well. Coupled with sediment entrapment, the effects on the hyporheic zone can be swift and devastating, and maintaining the hyporheic zone would be difficult (Brunke and Gonser, 1997). The restoration practices that are commonly used on rivers mostly involve structure additions for improving fish habitats, but most do not take into account the importance of the hyporheic zone. The pool-riffle system, which can have a meandering morphology might not contain the necessary structures essential for proper hyporheic exchange when anthropogenically altered. Some suggestions for hyporheic zone management on pool-riffle channels might be to prevent sediment from reaching interstitial spaces, but also to provide a varied range of sediment sizes so different hyporheic conditions can exist.

The hyporheic zone plays a key ecological role in the healthy functioning of a pool-riffle channel, and management strategies should involve not just stream connectivity, but hyporheic zone and exchange connectivity as well. However, because the hyporheic zone is difficult to

study and is not well understood, there needs to be more research on its geomorphological and ecological function before properly implementing better management techniques.

3.1. Biological Interactions

To better understand the ecological and hydraulic function of the hyporheic zone, it is important to gain a better understanding of some species that interact with hyporheic processes. The sea lamprey (*Petromyzon marinus*) and Atlantic salmon (*Salmo salar*) create a spawning nest called a redd. The sea lamprey and Atlantic salmon construct redds by moving cobbles to form a pit and mound structure, with the pit upstream from the adjacent cobble mound. These structures are commonly found miles upriver when these two species swim into freshwater to spawn.

3.1.1. Sea Lamprey (Petromyzon marinus)

Sea lamprey are an anadromous fish species that are commonly found along the Atlantic coast from Florida to the Gulf of St. Lawrence. Lamprey are a cartilaginous fish without true jaws, and instead have a large circular mouth with rows of teeth. A lamprey's mouth provides powerful suction when attaching to prey and constructing their spawning redds in freshwater. When spawning in freshwater the lamprey loses its ability to see, so it relies on its other senses during this period. Lamprey redds consist of a pit and mound; the mound is constructed when the lamprey suctions cobble sized rocks into a pile (Figure 3.2 and Figure 3.3). The pit is a result of the excavation of cobbles to build the mound. When the lamprey eggs hatch, they rely on the interstitial spaces in the mound for protection, oxygen, and nutrients. These requirements are transported into the mound by hyporheic flow into the redd.

Figure 3.2. A sea lamprey spawning on the Blackledge River in Connecticut. (Photo by D. Thompson).

Figure 3.3. A lamprey redd (Photo by G. Susac, OASIS).

3.1.2. Atlantic salmon (Salmo salar)

Atlantic salmon are an endangered, anadromous fish species found in Down-east Maine to the south of Greenland to Europe and Iceland. In the United States, Atlantic salmon are only found on the Dennys River, East Machias River, Machias River, Pleasant River, Narraguagus River, Ducktrap River, Sheepscot River, Cove Brook, Penobscot River, Androscoggin River, and Kennebec River (NOAA Fisheries, 2015), although some Atlantic salmon survive in the Connecticut River and Merrimack River as stocked fish. However, Atlantic salmon historically had a much larger southern range to the Long Island Sound (NOAA Fisheries, 2015). When spawning, suitable river habitats consist of gravel or cobble in riffle areas. Atlantic salmon face upstream and use their powerful tails to create their redds. The tail movement excavates the pit to form the mound of medium sized cobbles. The pit is created as a result of the downstream movement, and fine sediments are sorted with the largest particles and cobbles moved to the mound, while the finer particles end up downstream (Figure 3.4 and Figure 3.5). A typical salmon redd is generally larger than a lamprey redd. When the salmon eggs hatch in March or April they become fry. They remain in the gravel for about six weeks, and rely heavily on the redds for protection, dissolved oxygen, and nutrients: a result of hyporheic flow in the redds.

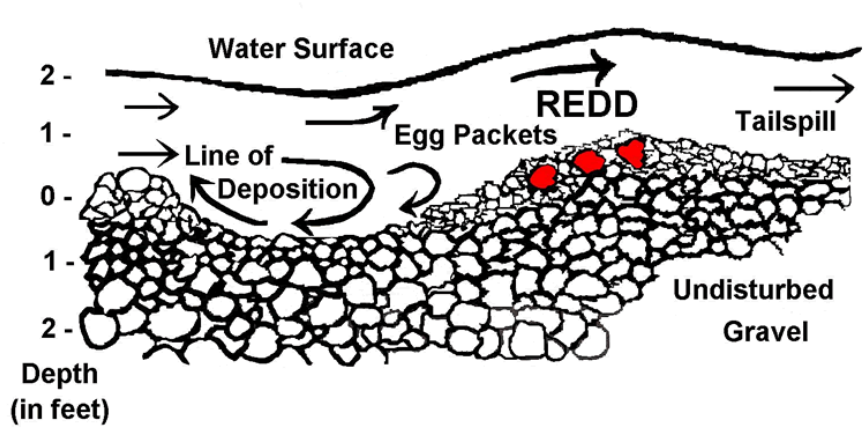

Figure 3.4. Diagram of a redd (Washington Department of Fish and Wildlife).

Figure 3.5. A Salmon redd on the Narraguagus River in Maine. (Photo by D. Thompson).

The process of hyporheic flow provides a lot of useful benefits for organisms that rely on the exchange for nutrients and DO. Like most aspects of a riverine system, hyporheic flow is very fragile process that can be easily disrupted. Hyporheic flow processes within lamprey redds likely provide similar benefits to lamprey eggs.

4. Methods

4.1. Study Area

The goal of the field study was to examine hyporheic flow processes at lamprey redds in-situ on the Blackledge River, Marlborough. The Blackledge River is 26.4 km long and is a tributary of the Salmon River, with a drainage basin of 3.88×10^8 m^2. The location of the site on the Blackledge River is: 41.577424°, -72.426456° (Figure 4.1; Figure 4.2). A salinity reader, recorded by video camera, and a saline injection apparatus were used to record velocity moving through several redds on July 8th, 2016. Redds were also measured for size, depth, and sediment size and averaged for an approximate size for a typical lamprey redd from June 8th and 9th, 2016. The location data for these redds can be found in *Appendix A*.

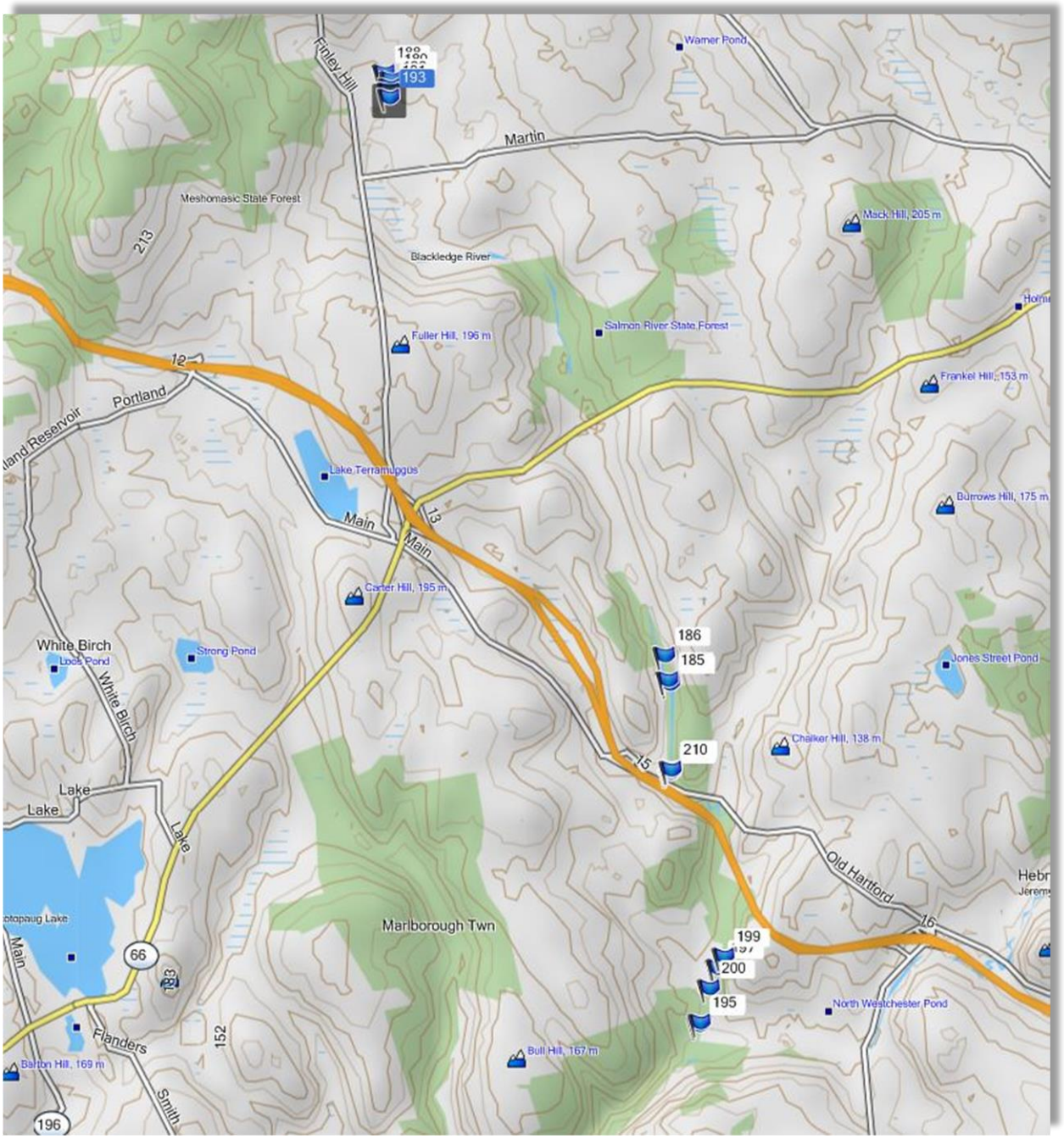

Figure 4.1. The location of all lamprey redds that were measured (Photo by D. Thompson).

An artificial redd was constructed in a recirculating flume using the average dimensions and sediment size obtained from lamprey reds in the Blackledge River. The flume house at Connecticut College, New London, Connecticut is 6.0 m by 0.5 m. The redd constructed within

the flume was observed using an acoustic Doppler velocimeter to measure surface flow velocity above the redd at different discharges using the Froude number. Then the data was compared to analyze areas of different pressures to investigate where hyporheic flow was taking place.

4.2. Saline Injections

The salinity probe was used to quantify hyporheic flow on the Blackledge River site: 41.577424°, -72.426456° (Figure 4.2). Hyporheic flow at two lamprey redds were measured in terms of salinity per unit time (ppm/s). The salinity probe measured salinity in parts per million (ppm). Saline injections of 3% (30,000 ppm) salt content or 30 g/L were delivered with a hollow metal rod, a plastic tube and a syringe containing the saline solution (Figure 4.3; Figure 4.4). These three items were connected together so it resembled an extended syringe. The metal tube was tapered at one end to allow for easy insertion into the bed (Figure 4.5). Then a small hole was punched through the tube at 2 cm from the bottom to allow the saline solution to pass through (Figure 4.4).

A measuring tape was laid 3-m down the approximate center of the redd parallel to the direction of the surface flow. The tape was not always straight because the flow moved differently over the redds. For example, large cobbles forced the flow laterally in some spots, causing the direction of the flow to move. At the beginning of each trial, saline injection rod distance, salinity probe distance, base salinity, rod depth, and salinity probe height were recorded (Figure 4.5). The redd mounds, pits, and sides were measured for hyporheic velocity. The height of the probe was kept 4.5 cm above the bed. The injection syringe was inserted 10 cm below the bed. The depth of the saline insertion point was kept constant at 10 cm into the bed for every trial, and the same volume (60 cm^3) of solution was inserted in a methodical way each time.

Injection rates were kept constant for each test. The time of the injections and recording was 30 seconds for each test. Only one side of the redd was tested, as it was assumed that the redds are generally symmetrical in behavior. The base of the pit, tail-spill, top of mound, rise in mound, and center of pit were probed for hyporheic flow in two redds. However, distances from those points were recorded at 10-cm intervals.

To accurately represent the fluctuation of salinity, a video camera was used for the duration of each injection time (Figure 4.3). The salinity (ppm) was recorded by an underwater camera, which taped the rise, peak, and fall of the salinity moving throughout the redds. A total of 30 trials for two redds were recorded. This data was then visually analyzed and recorded in Grapher to create salinity vs. time graphs. A secondary analysis was conducted by utilizing a concentrated dye solution. The dye was injected into the bed in a similar fashion as the salinity syringe, but only 10 injections took place in each redd because of retention of the dye in the redds. The purpose behind this investigation was only to visually confirm water flow through the redd.

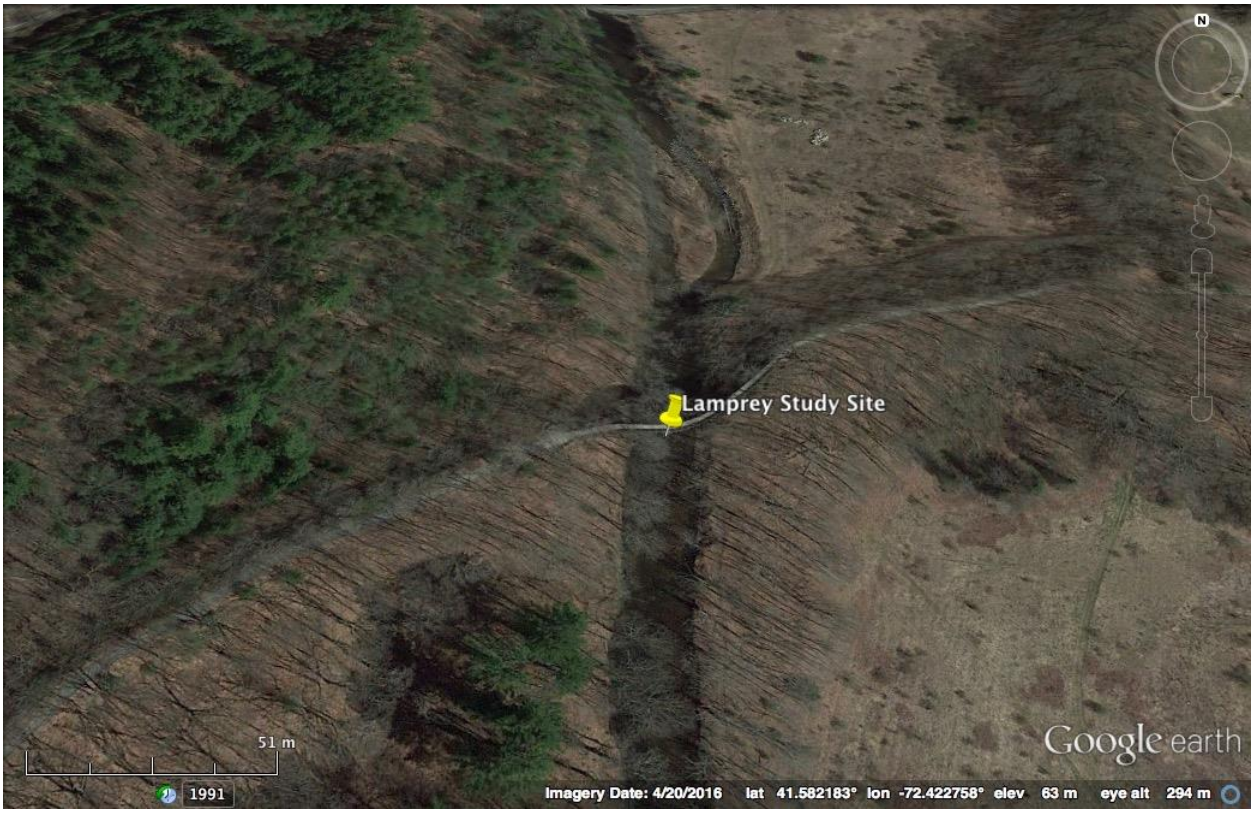

Figure 4.2. The study site for the saline injections into the sea lamprey redds

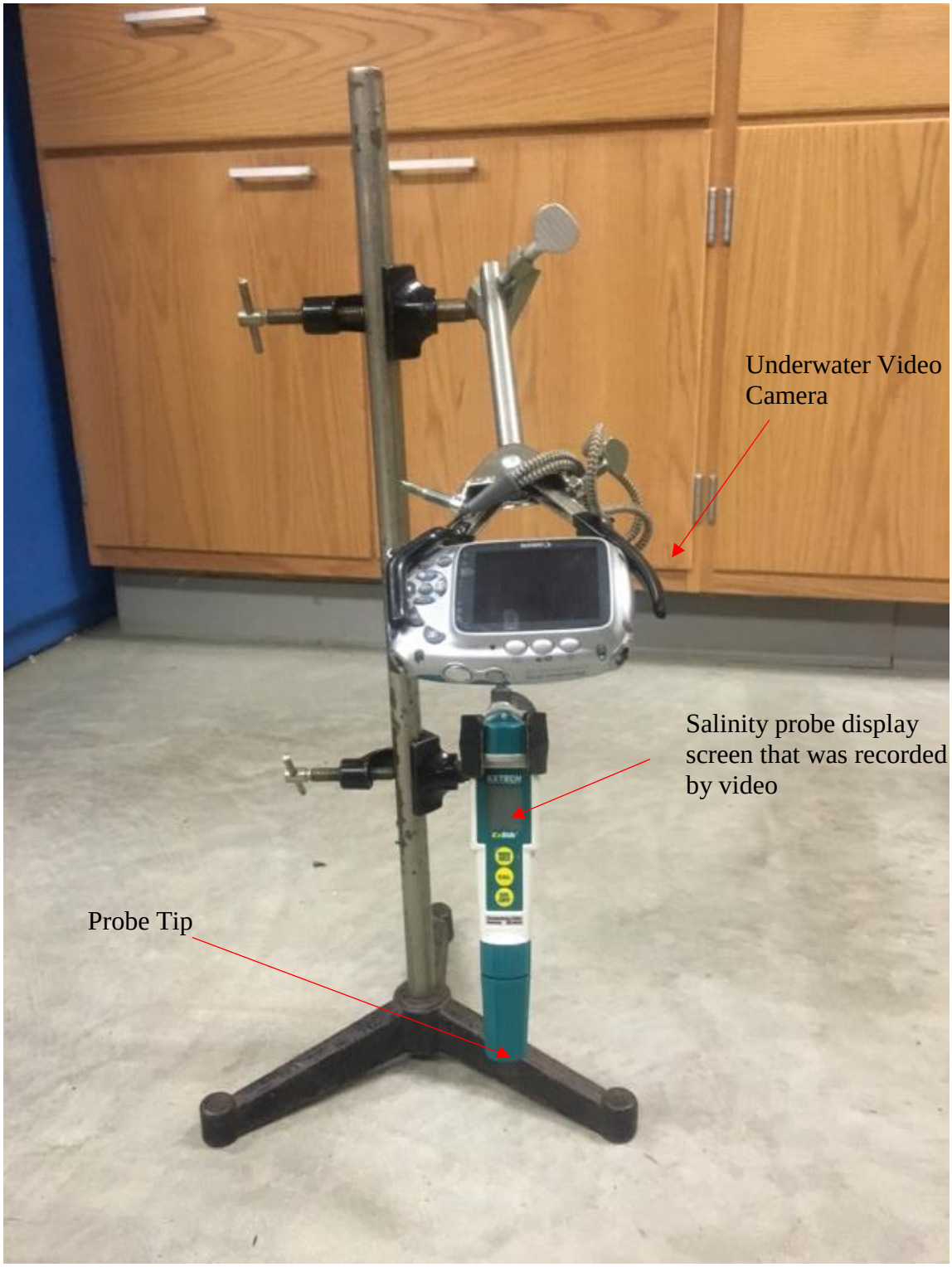

Figure 4.3. The salinity probe setup with recording device.

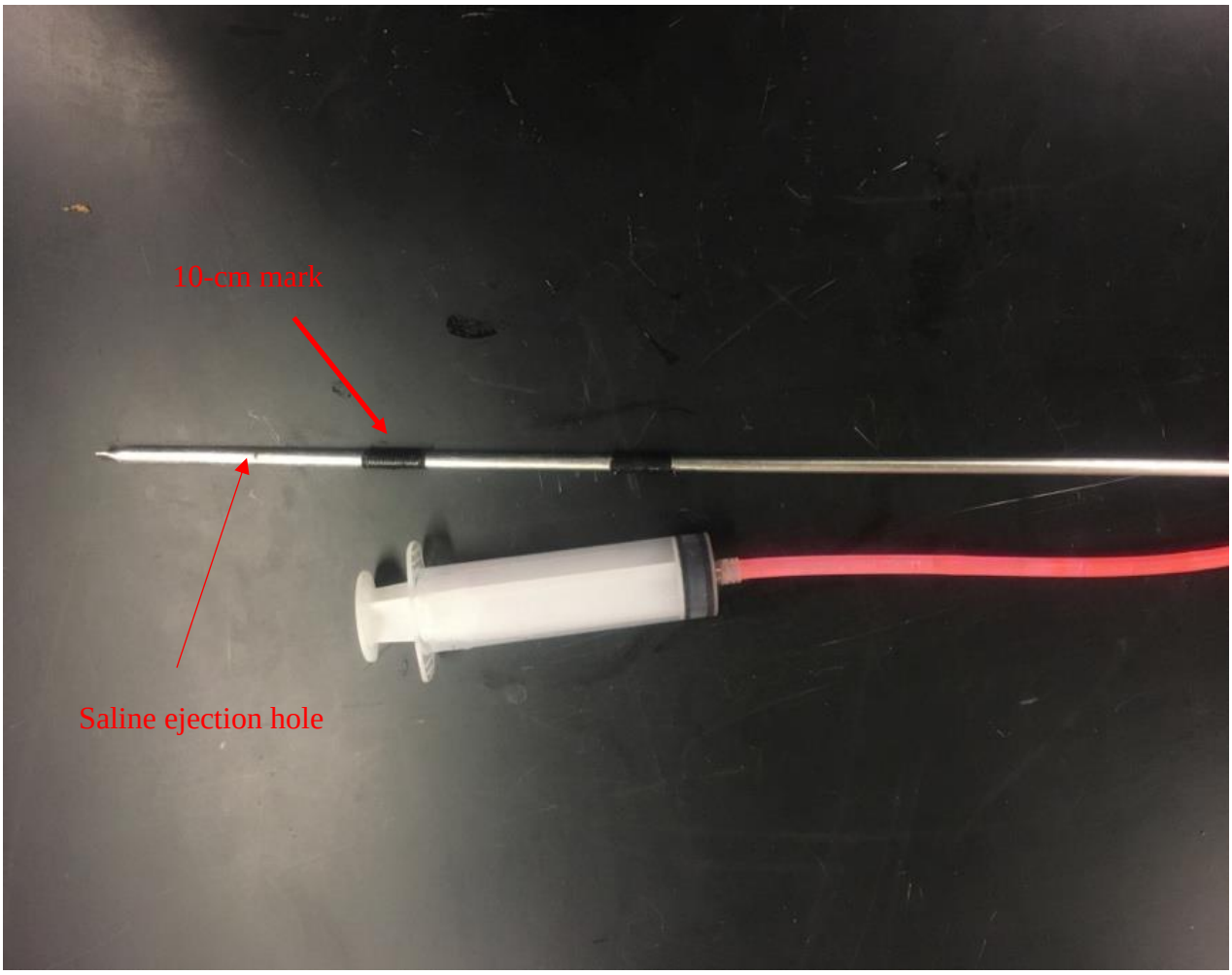

Figure 4.4. The syringe used to inject the saline solution. The first black tape (arrow) on the metal rod represents the 10 cm mark, which was the depth of the injection into the bed.

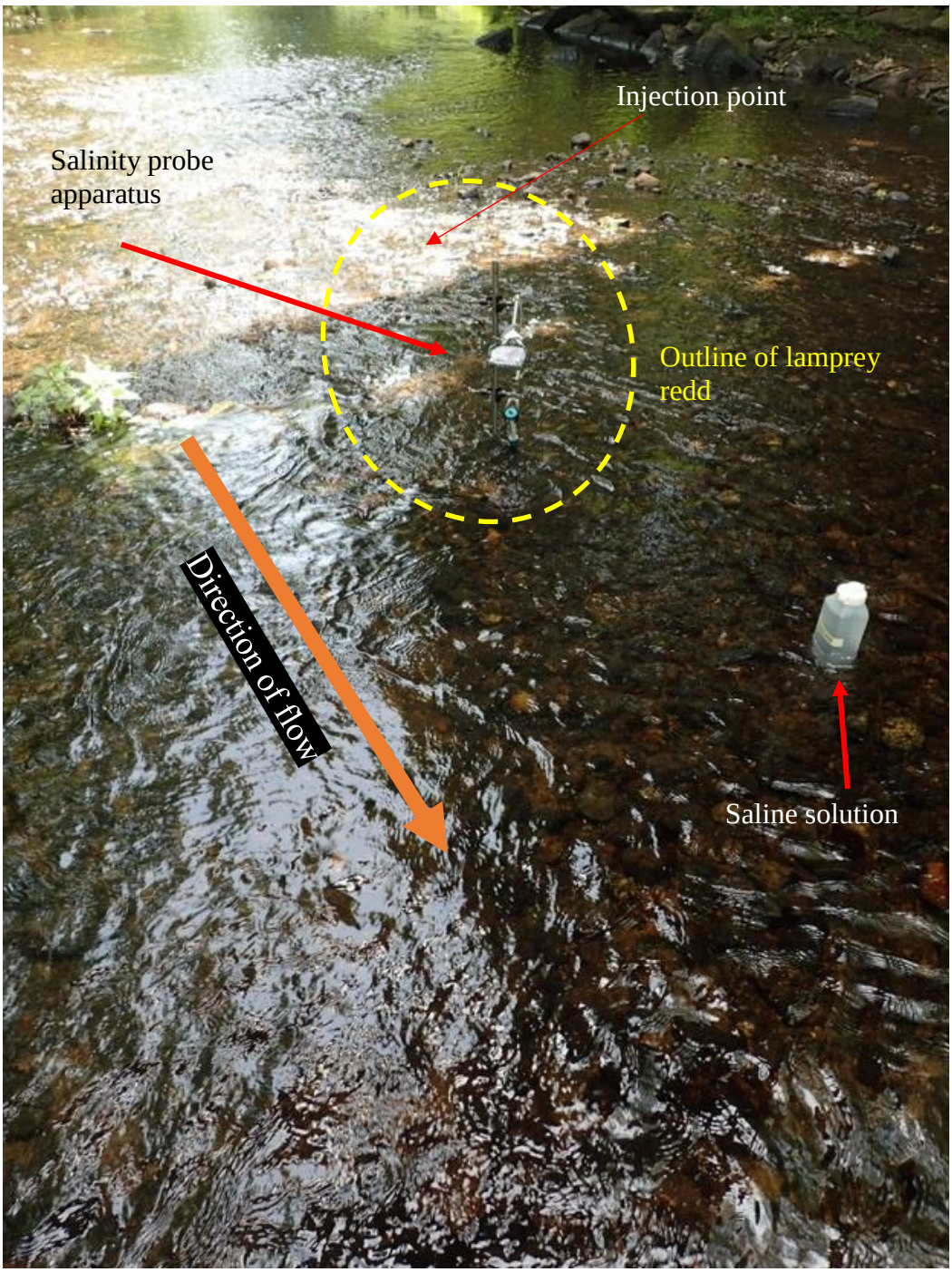

Figure 4.5. The salinity probe and the saline solution bottle in action in the Blackledge River.

4.3. Lamprey Redd Longitudinal Cross Sections and Velocity

Longitudinal cross sections of eight lamprey redds on the Blackledge River were measured as well as 60% surface flow velocity measurements (m/s) using an auto level and a Marsh McBirney Flow Meter, respectively. The sampling data was collected on June 1st (107 cfs), 2nd (65 cfs), 7th (103 cfs), 10th (51 cfs), and 13th (62 cfs) (Figure 4.7). The redds were sampled 2-m upstream, at the pit, at the mound, and 2-m downstream. This data was useful for examining average velocities of the redds, which would be compared to the velocities found at the constructed redd within the flume. The USGS data was used in combination with the Froude number to scale the redd to the flume (*See Section 4.5 Flume Measurements*).

4.4. Lamprey Redd Topography

Lamprey redds were surveyed using a TopCon GTS Laser Total Station on June 12th, 2016. A benchmark was set so accuracy could be determined and future datasets could be recorded. Each lamprey redd was measured systematically around its pit and mound. Cross sections of the bed stream topography were also measured 2-m upstream and 2-m downstream from each redd. The third cross section was measured directly over the redds. Data sets were downloaded and topographically analyzed using Surfer by creating isoline maps.

4.5. Flume Measurements

The sediment sampling of the eight lamprey redds was needed to obtain the average phi size of a lamprey redd. An artificial lamprey redd was created in the 6.0 m by 0.5 m flume and approximately scaled to 50% actual size using the average dimensions of the eight lamprey redds and the average phi sizes. Sediments were sorted into 50% phi sizes of those found on lamprey

redds in the Blackledge River because the flume can only fit a scaled redd. The recipe for the sediment was based on approximately 50% surface composition and 50% subsurface composition.

The sediment mix for the surface layer was obtained by taking several 5 gallon buckets and filling them with sediment from the Blackledge River. The sediment mix for the subsurface layer was created by using smaller sediments from the Blackledge River and gravel and sand from a nearby quarry. These sediments were mixed together and placed in the flume according to the percent they were found in the Blackledge River (Figure 4.6 and Table 4.1). A subsurface layer was created with small fines, gravel, and cobbles.

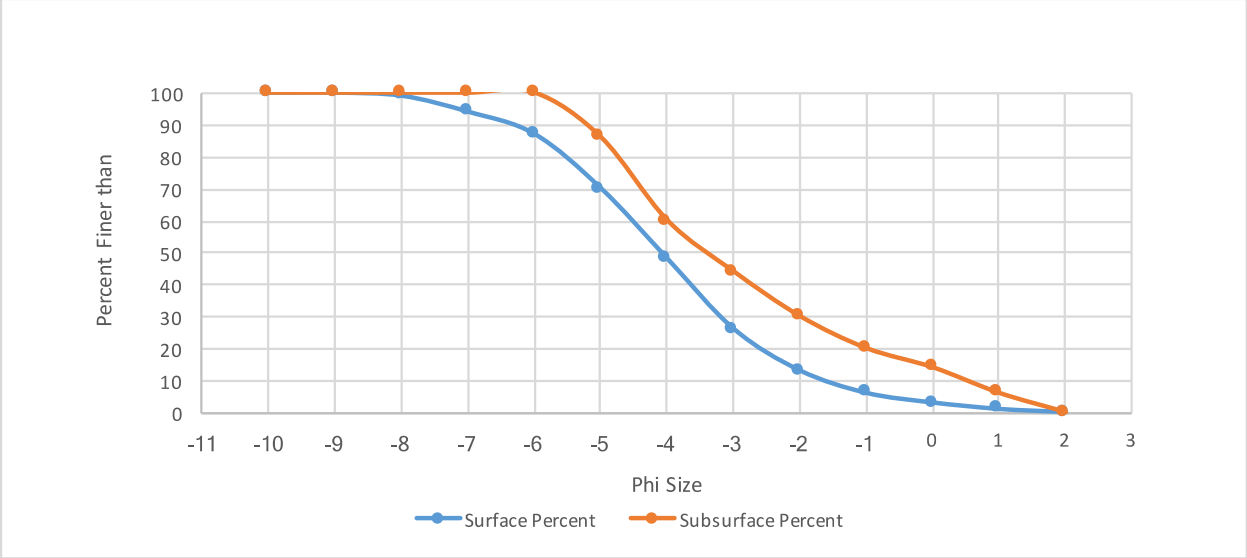

Figure 4.6. Sediment size distribution for the subsurface and surface sediments from the Blackledge River.

Table 4.1. Phi size and percent of phi sizes needed for each bucket for use in the construction of the artificial redd. The buckets column represents the amount buckets that needed to be filled with sediments to match.

Phi Size	Surface %	Subsurface %	Size (mm)	Size (in)	Buckets
2	0%	0%	0.25	S	
1	0%	0%	0.5	A	
0	3%	10%	1	N	
-1	3%	10%	2	D	1.3
-2	7%	10%	4	0.157	0.85
-3	13%	14%	8	0.315	1.35
-4	22%	16%	16	0.630	1.9
-5	22%	26%	32	1.26	2.4
-6	17%	14%	64	2.52	1.55
-7	13%	0%	128	5.04	0.65
-8	0%	0%	256	10.1	0
-9	0%	0%	512	20.16	0
-10	0%	0%	1024	40.31	0

Topographic stream bed and velocity data were collected in the flume from 250 cm to 350 cm from the head of the flume. The topography of this section consisted of the most river-like sediments, gravels, and cobbles. The cobble, gravel, and sediment placed in the flume was the same phi-size percent surveyed on the Blackledge River (Figure 4.7). The slope of the flume was set to the average slope of the Blackledge River along the sampled redd location, at 0.6%. Once the sediment was placed in the flume, several flume runs were implemented at high velocities to test the integrity of plain bed and to settle any loose sediments. The bed topography was measured with a point gauge in a grid pattern from the longitudinal distance of 250 to 350 cm in 5-cm increments, and latitudinal measurements occurred from 5 to 45 cm in 5-cm increments.

Measurements were scaled using the Froude number from the Blackledge River flows of June 6th, 7th, and 9th of 2016 (Equation 4.1). The 6th and 7th of June dates represent the potential spawning dates of lamprey on the Blackledge River (Figure 4.7). The 9th of June represents observed data and a sighting of a lamprey on its spawning redd. Discharge in the flume was scaled to the flume using approximate discharges recorded by USGS gaging station 01193500 on the Salmon River near East Hampton, CT (Figure 4.9; Equation 4.1). This is the closet gaging station to the Blackledge River, which is a tributary of the Salmon River.

$$F = \frac{V}{\sqrt{gD}} \qquad \text{(Equation 4.1)}$$

(where F=Froude number, V=velocity, g=gravity, and D=density)

The Froude number values were calculated for the field conditions that translated to the data from the recorded cfs dates from the USGS (Equation 4.1). The Froude numbers were then compared to the Froude number values that were collected at lamprey redds on the Blackledge River. The average depth upstream of the pits was used to scale the flume depth. The Froude numbers were converted to low, medium, and high flows that would be found on the river. These scaling calculations established that the artificial redd would be made at a flow rate of 19.5 l/s in the flume which corresponds to the Salmon River discharge of 100 cfs. The calculations for the Froude number values can be found in *Appendix B*. The flood simulation for the Blackledge River would be 32.4 l/s at approximately 25 cm of water depth in the flume. This flow would be

the most likely time the lamprey came upstream to spawn (Figure 4.7). The low flow of the Salmon River would be scaled to 11.7 l/s in the flume.

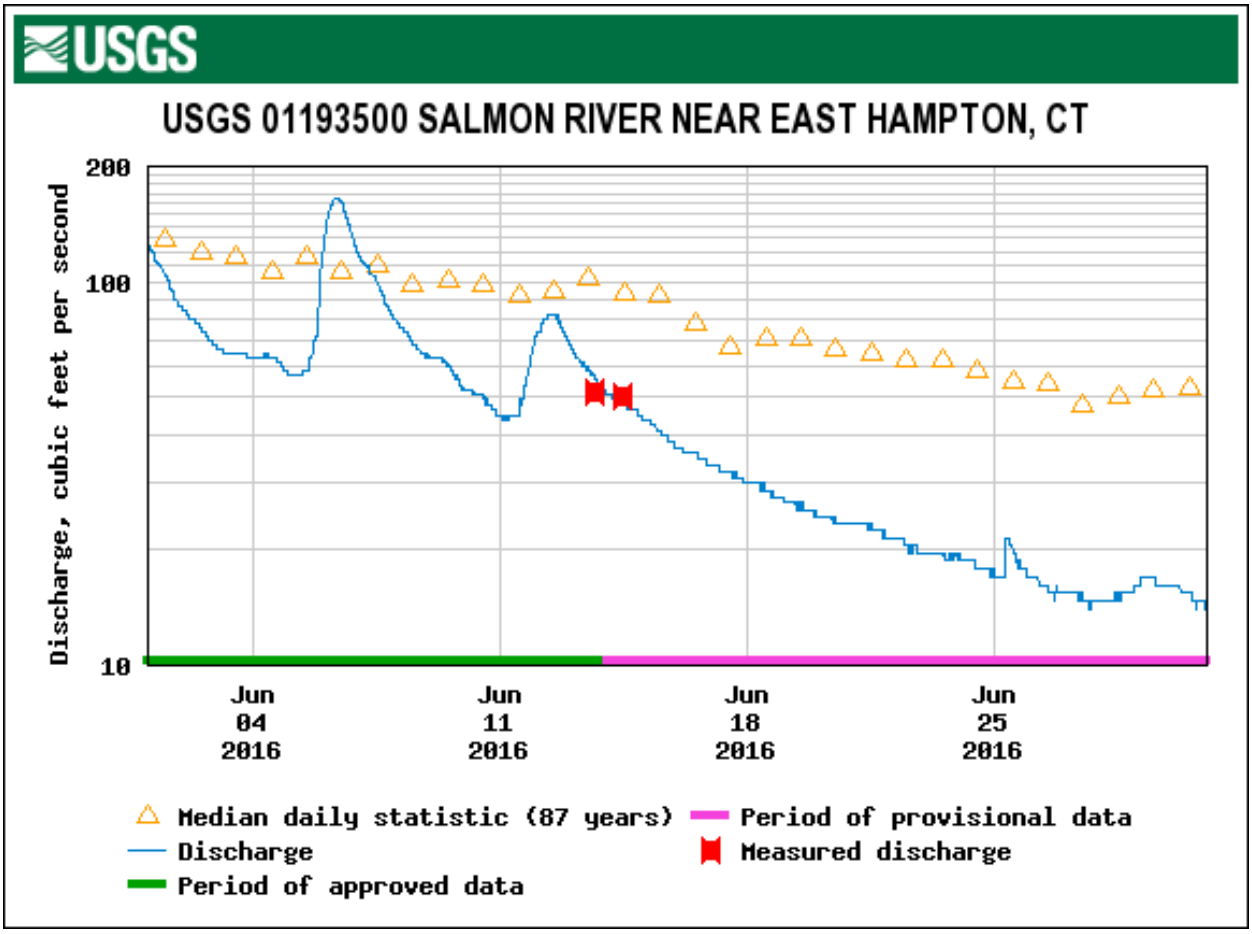

Figure 4.7. A hydrograph for the Blackledge River from June 1st-30th. This data was used to scale discharges in the flume.

Figure 4.8. The two plates, that represent the average size of the redds, show the placement of the redd in the flume.

Figure 4.9. The final created product of the redd in the flume with the templates used in their construction.

The artificial lamprey redd was constructed in water flowing at 19.5 l/s using metal templates (Figure 4.9; Figure 4.10). The templates were created using the average width and length measurements from eight redds (Table 4.2). The redd was constructed in a "blind" manner to replicate the lamprey's situation during redd construction. Without looking, rocks were moved from upstream to downstream by hand and by only moving one rock at a time to create a redd within the scaled values. When the flow was shut down, it was determined that the scaled redd was not large enough the first time compared to the area of the metal templates. As a result of this, the flow was resumed and the redd was constructed to be slightly bigger under the same flow conditions. The goal was to replicate a real redd as much as possible. Special attention was paid to the size of the pit and the mound, and the height and depth were roughly scaled to be replicas of the redds observed in the Blackledge River. The pit was approximately 5.5 cm deep, which was close to the scaled value of 5.65 cm (Table 4.2). The scaled value of 2.1 cm for the mound closely resembled the actual value of 2.38 cm (Table 4.2). The process was fine-tuned several times in order to represent a realistic redd.

Table 4.2. The average parameters for the creation of the redd in the flume

Lamprey Spawning Redds	Pit Depth (cm)	Pit Width (cm)	Pit Length (cm)	Mound Height (cm)	Mound Width (cm)	Mound Length (cm)
Mean	11.31	43.13	55	4.75	46.43	42.14
Standard Deviation	4.12	10.33	16.48	3.05	12.82	13.18
Scaled 50%	5.66	21.56	27.5	2.38	23.21	21.07

Once the model redd was constructed, velocity measurements were taken at the three scaled discharges using a SonTek acoustic Doppler velocimeter (ADV). Measurements were taken from 250 to 350 cm at 10-cm longitudinal increments. Measurements were taken from 5 to 45 cm at latitudinal 10-cm increments. To create a more precise 3-D field at the location of the

redd with additional measurements were taken longitudinally from 270 to 320 cm at the 20 cm and 30 cm widths. Measurements were taken for a 2-minute duration with the ADV at a 60% depth of the 19.5 l/s discharge level. This height above the bed stayed the same throughout the duration of the experiment so the ADV measured the same 60% depth point at all three discharges.

4.6. Computational Analysis

Topographical maps of the bed before and after the redd construction were created using Surfer 8. This data was used to analyze the relationship between topography and velocity. The ADV data was then analyzed using WinADV and SonTek software to remove inaccurate data points and create more precise data. The points were then filtered using Nortek software where the Signal to Noise Ratio (SNR) was used to remove data points with less than 0.85 dB correction (Thompson, 2006). A Gaussian low-pass filter was also used to filter the data and account for problems associated with aliasing (Thompson, 2006). The data points were then averaged to create a velocity field at the measured points within the flume.

The RMS values (Root Mean Squared), created by the ADV velocity measurements were used to create turbulent kinetic energy values (TKE) (Equation 4.2).

$$k = 0.5 \cdot p \cdot (\text{RMS } V_x^2 + \text{RMS } V_y^2 + \text{RMS } V_z^2) \qquad \text{(Equation 4.2)}$$

The RMS V_x, RMS V_y, and RMS V_z are the root mean square values for the downstream, lateral, and vertical components of the flow that were obtained in a 3-D field by the ADV, and *p* is fluid density. The TKE values were created for the x, y, and z planes. The TKE values were used to

produce maps that illustrate zones with high turbulence production (fluid motion to thermal energy), and these areas of turbulence were used to extract information on areas of upwelling, downwelling, and lateral movement. The aim of this information was to deduce areas of low and high pressure zones to predict the amount of hyporheic flow taking place. This is based on the assumption that the low and high pressures push water through the redd and into the mound. The TKE data, velocity values, and vertical velocity (Vz) mean values were scaled to create arrows on post-maps, which overlay the underlying topographical isoline maps. The velocity data x and y values were translated through the Pythagorean theorem to produce the magnitude and direction of the two combined into a single vector. The length of the arrows corresponds to the velocity, and the angle dictated the direction of the flow. The underlying isoline data was TKE data. The downstream and cross-stream V_z-isolines were transformed to magnitude or vertical velocity on the post-maps.

The methods were designed to produce an experiment that would help illustrate the hyporheic processes at work within lamprey redds. The topographical surveys, longitudinal surveys, saline injections, phi size distribution, and scaled redd experiment were all designed to work in conjunction and provide an outline to hyporheic methods. Overall, the combined methods were expected to provide a representation of hyporheic flow processes and flow movement within an average lamprey redd.

5. Results

The results from the combination of the studies indicate that the pit and mound force vertical velocity patterns over the mound and create strong upwelling and large localized TKE values. TKE values are always higher over the mound, and the areas of strong upwelling and downwelling increase with stage. The saline injection study suggests that there is a stronger correlation in readings just before the mound, which indicates potential travel through the mound. The injections further upstream suggest longer residence times and more input of the solution into the bed.

5.1. Redd Topography and Velocity

The topography of the redd is lowest in the pit and highest at the mound down the center line of the redd. The velocity for the 11.7 l/s flow rate increases through the pit and decreases over the mound and immediately downstream of the mound, most apparently down the center line of the redd (Figure 5.1). At the second stage the velocity for the 19.5 l/s flow rate increases through the pit and decreases over the mound and immediately downstream of the mound. These results are most obvious down the center line of the redd (Figure 5.2). The velocity for the 32.4 l/s flow rate increases through the pit and decreases over the mound and immediately downstream of the mound, the pattern is most evident down the center line of the redd (Figure 5.3).

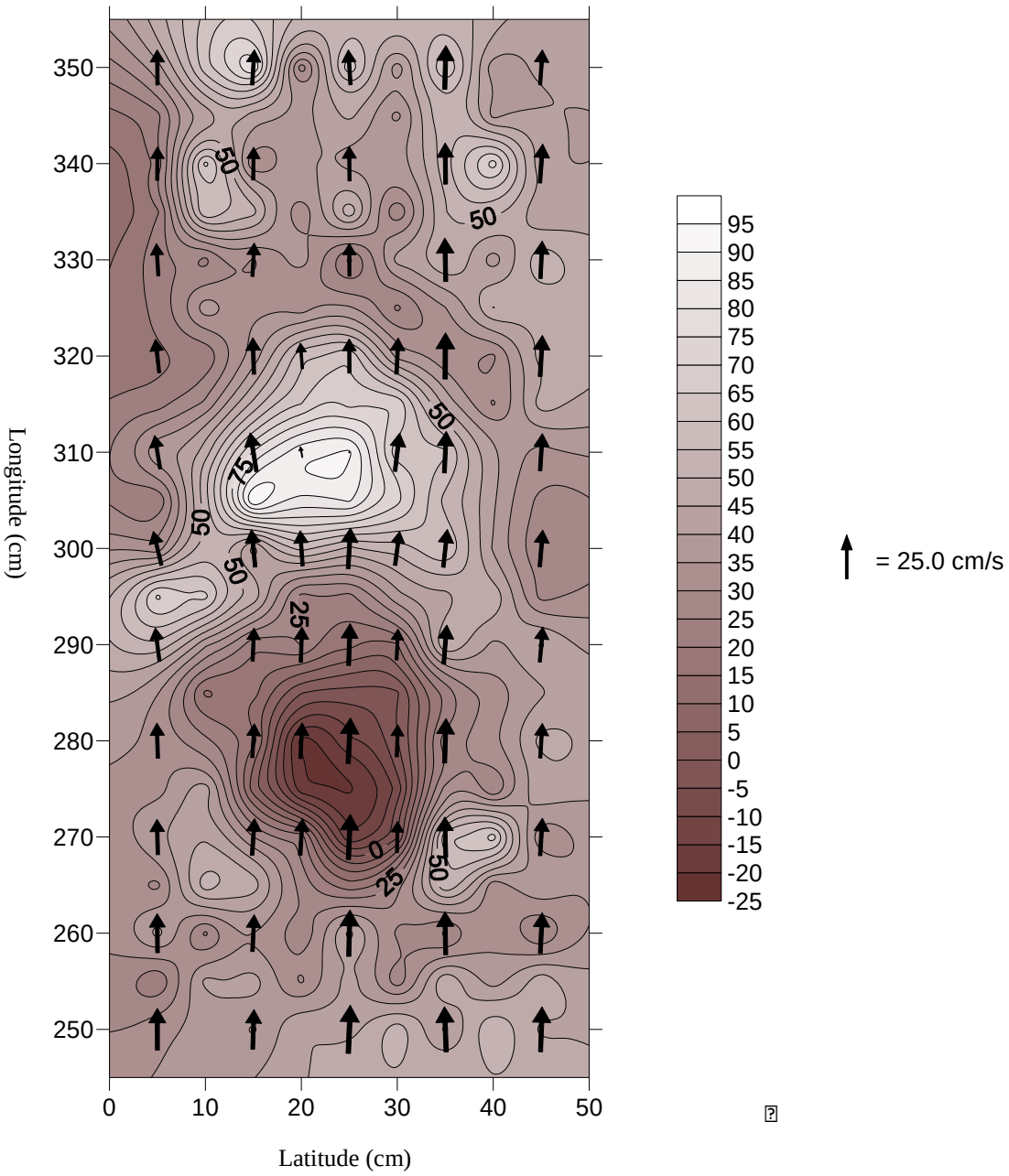

Figure 5.1. The topography isolines of the constructed redd with arrows representing scaled velocity at a stage of 11.7 l/s. The arrow illustrates the scale for velocities (cm/s).

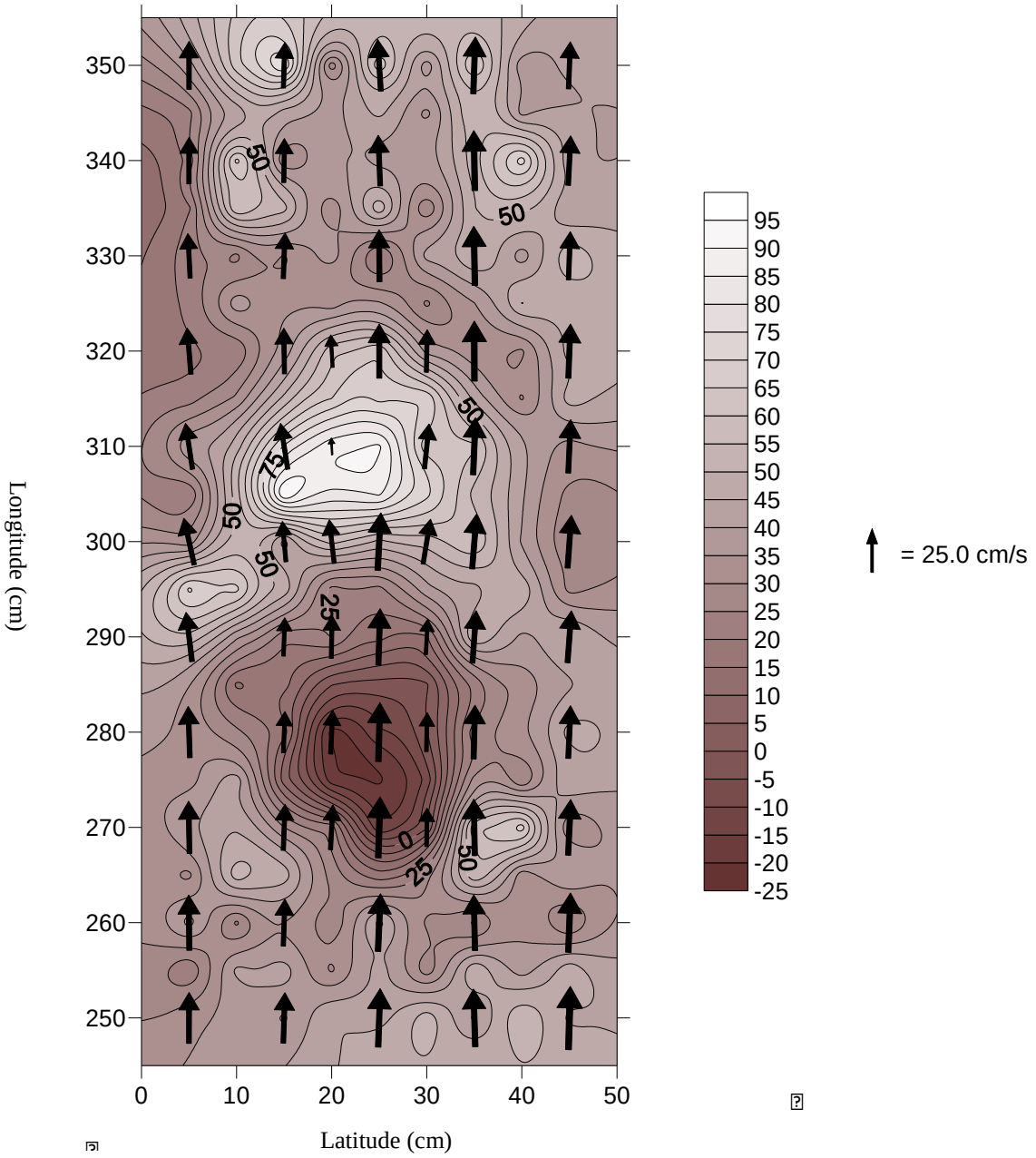

Figure 5.2. The topography isolines of the constructed redd with arrows representing scaled velocity at a stage of 19.5 l/s. The arrow illustrates the scale for velocities (cm/s).

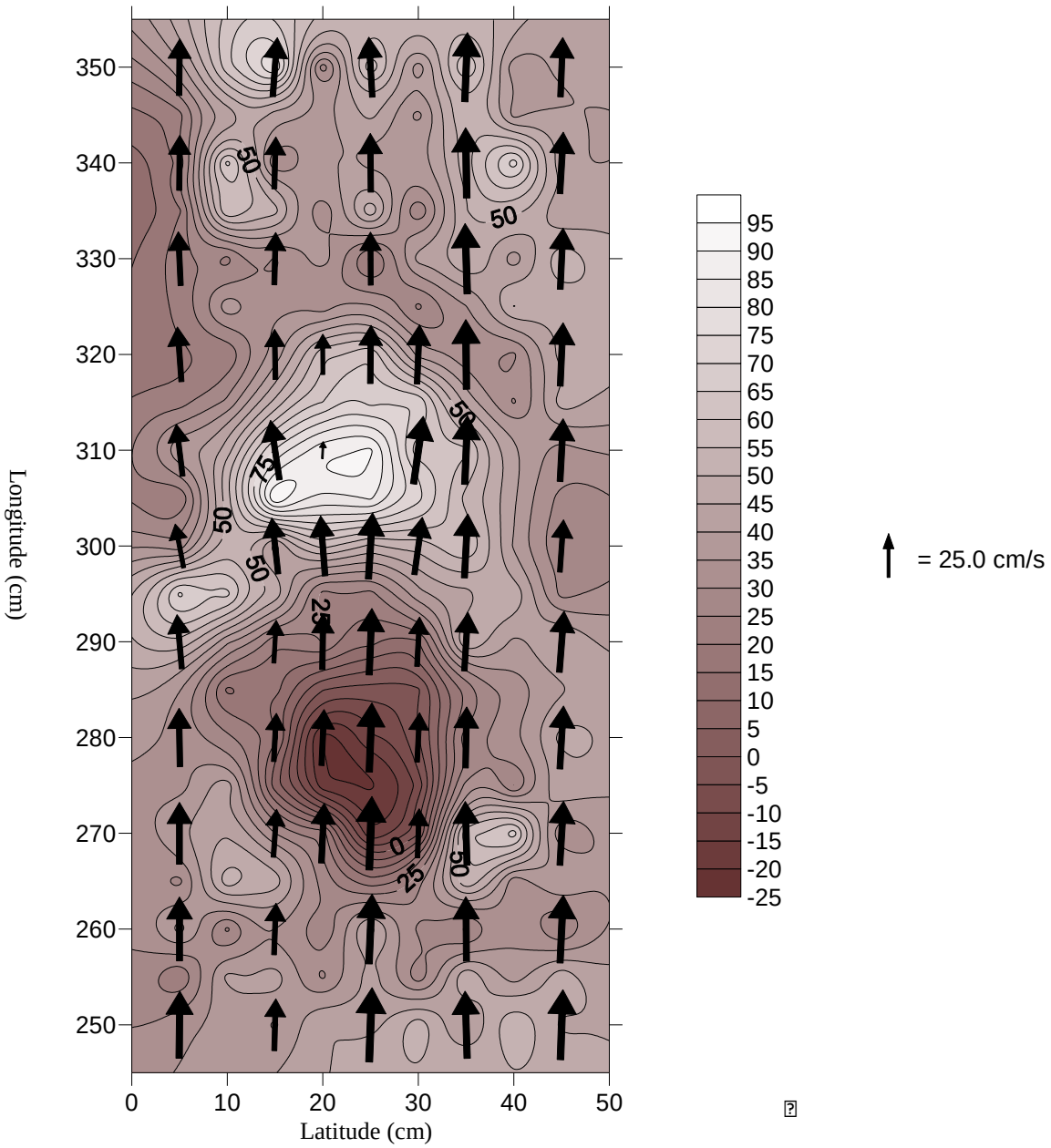

Figure 5.3. The topography isolines of the constructed redd with arrows representing scaled velocity at a stage of 32.4 l/s. The arrow illustrates the scale for velocities (cm/s).

5.2. Redd Longitudinal Profiles

Lamprey redd 1 has a much more variable water surface profile than redd 2, with a steeper mean gradient (Figure 5.4; Figure 5.5). Redd 1 has a shorter pit to mound distance than redd 2, and the tail spill is rougher. The water surface slope also decreases after the top of the mound as the slope of the mound decreases.

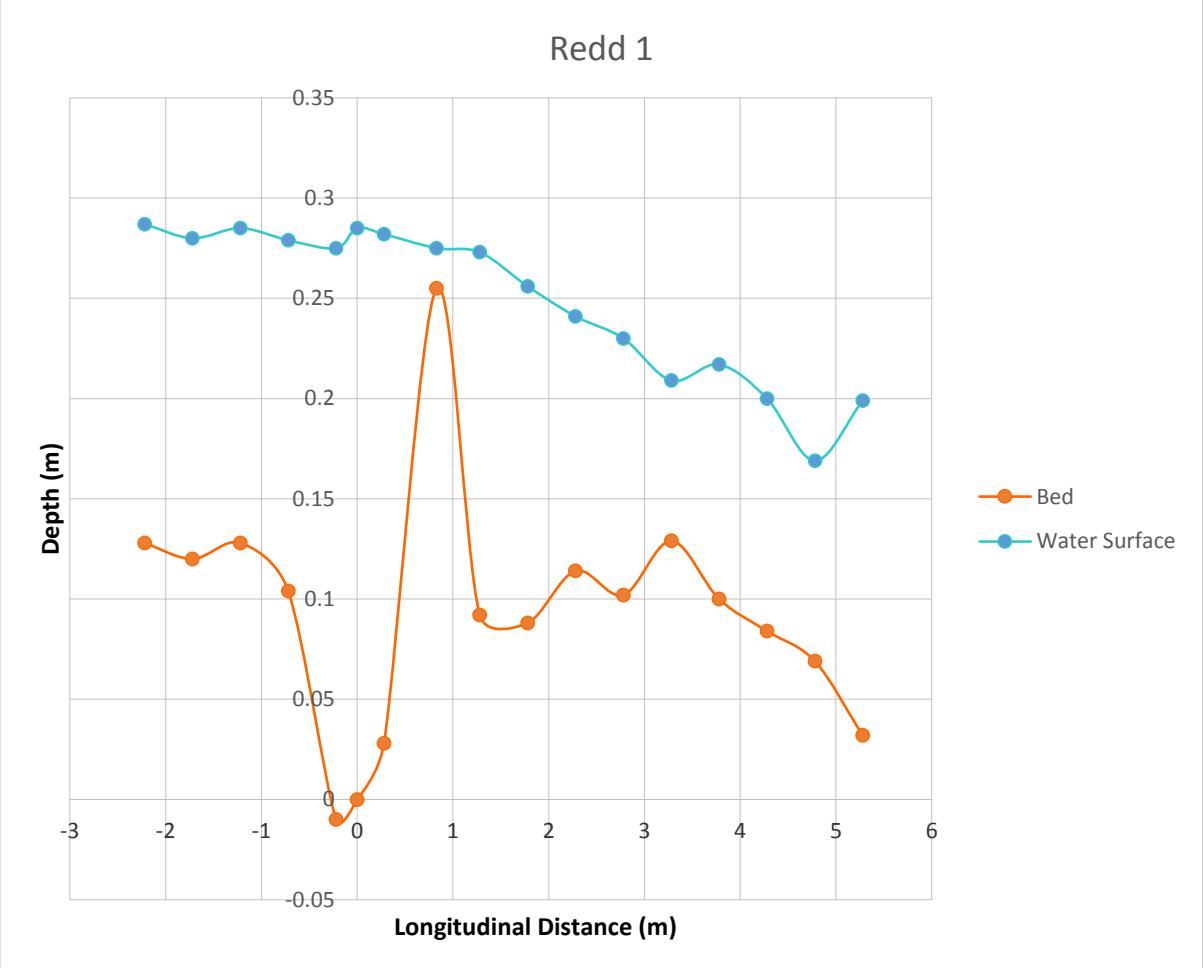

Figure 5.4. The longitudinal topographic profile of the first redd and the water surface height.

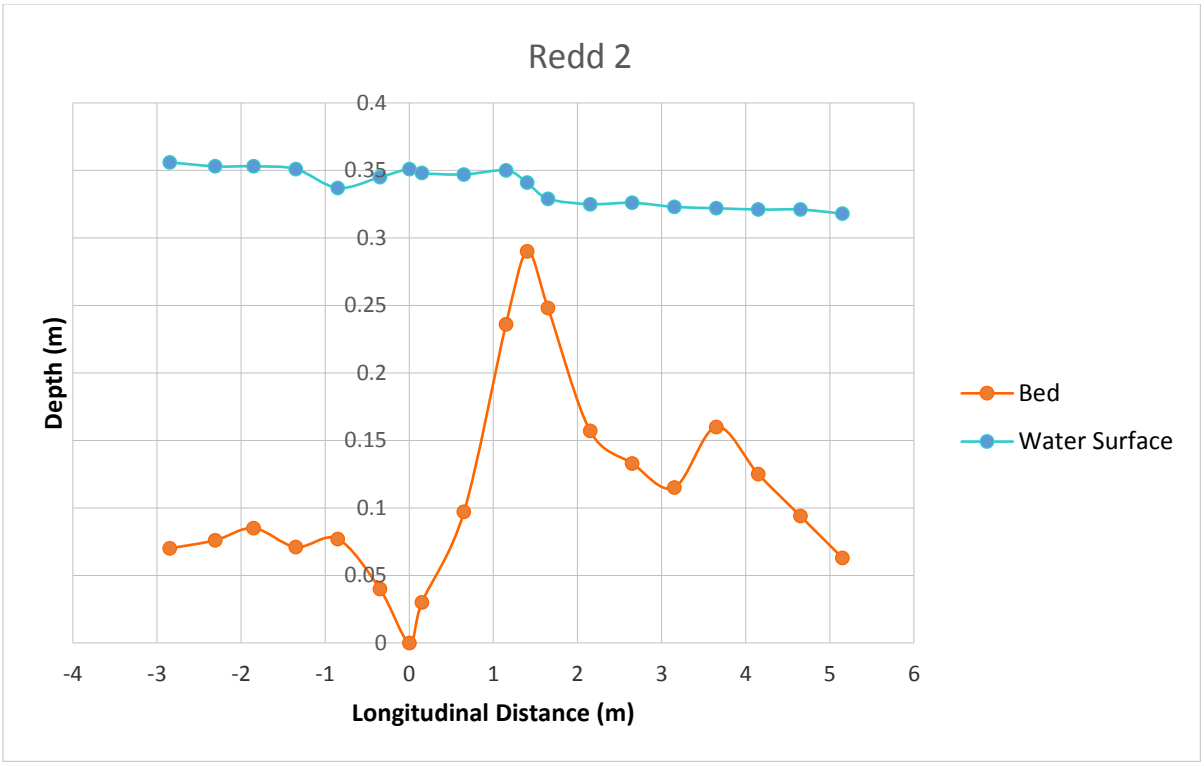

Figure 5.5. The longitudinal topographic profile of the second redd and the water surface height.

5.3. Mean Vertical Velocity

The mean vertical velocity for the flume discharge of 11.7 l/s was lowest before the pit and highest over the mound. The velocity was fastest down the center of the redd. The velocity arrows indicate lateral movement around the redd at the 5-cm latitudinal line. Velocity was lowest immediately downstream of the mound at the 310-cm latitudinal mark (Figure 5.6).

The mean vertical velocity for the flume discharge of 19.5 l/s was lowest before the pit and highest over the mound, similar to the low flow rate. The velocity was fastest down the center of the redd. The velocity arrows indicate lateral movement around the redd at the 5-cm and 45 cm latitudinal lines. Velocity was lowest immediately downstream of the mound at the 310-cm longitudinal mark (Figure 5.7). Similar but exaggerated patterns exist between the low and medium flow rates.

The mean vertical velocity for the flume discharge of 32.4 l/s was lowest before the pit and highest over the mound, similar to the low and medium flow rates. The velocity was fastest down the center of the redd. The velocity arrows indicate lateral movement around the redd at the 5-cm, 35-cm, and 45-cm latitudinal lines. Velocity was lowest immediately downstream of the mound at the 310-cm longitudinal mark (Figure 5.8). Similar but exaggerated patterns exist between the low and medium flow rates and the high flow.

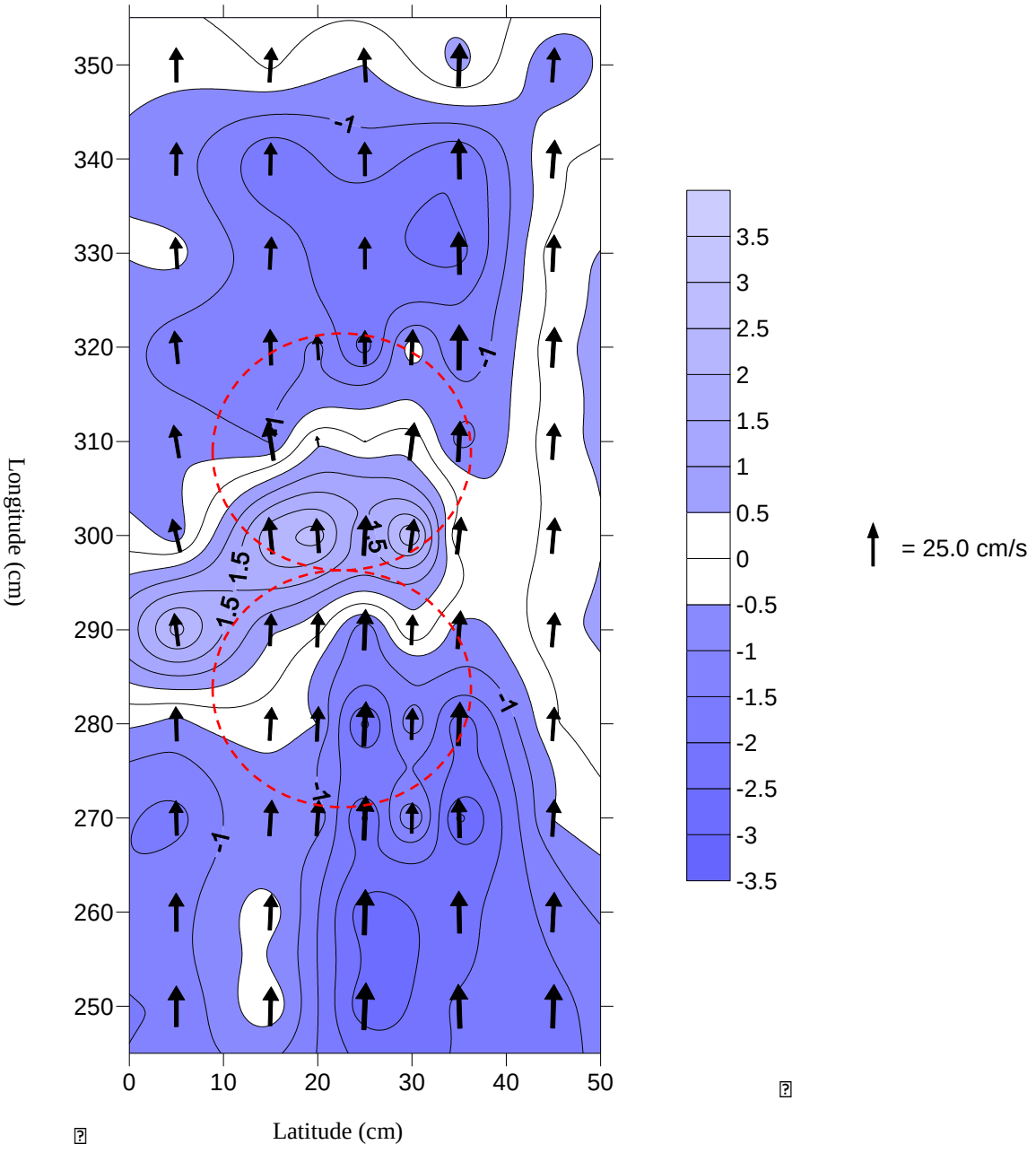

Figure 5.6. The average vertical velocity represented by isolines at a stage of 11.7 l/s with arrows indicating scaled velocity. Upwelling is represented by positive values, and downwelling is represented by negative values. The dashed red circles represent the approximate location of the upstream pit and the downstream mound. The white areas indicate values near zero. The arrow illustrates the scale for velocities (cm/s).

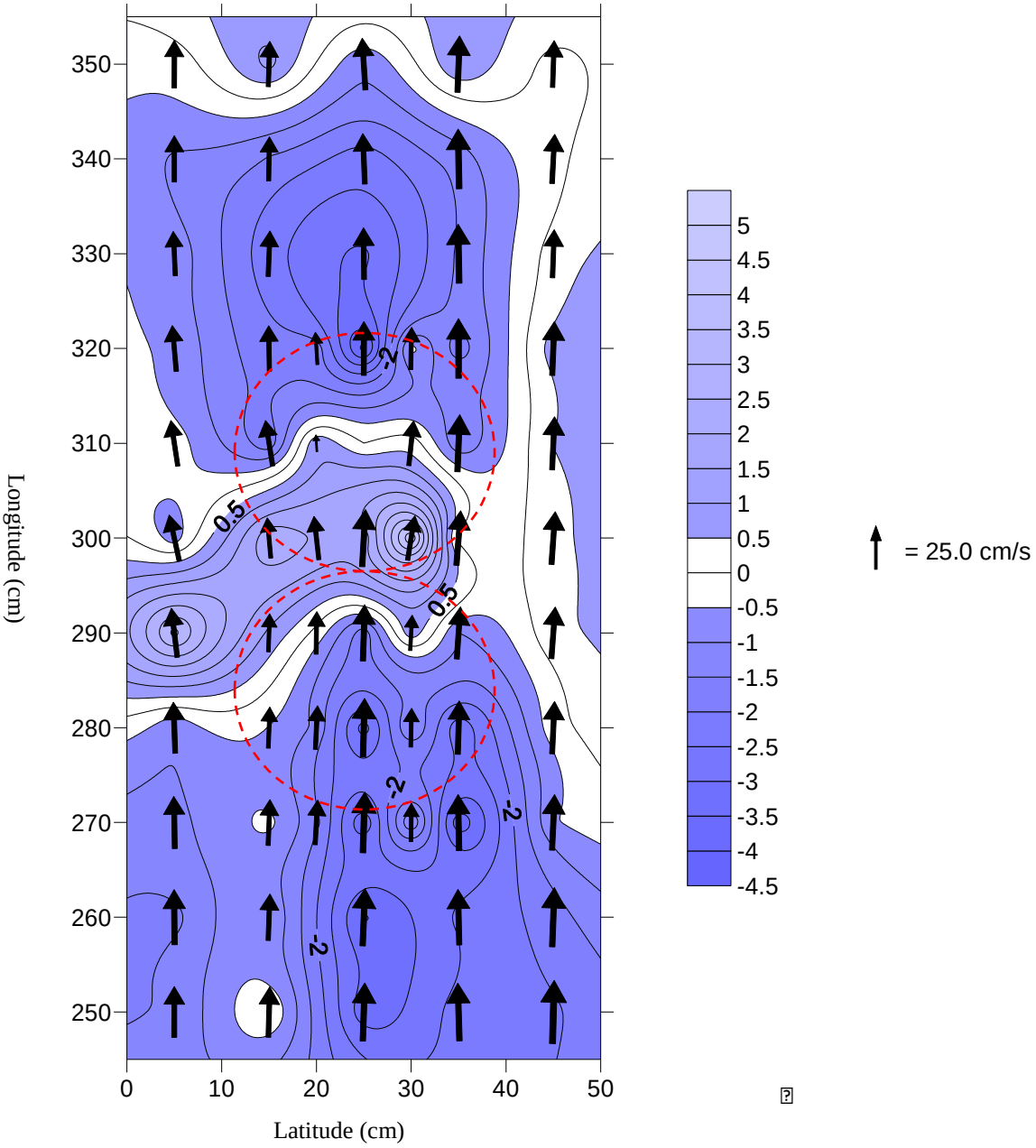

Figure 5.7. The average vertical velocity represented by isolines at a stage of 19.5 l/s with arrows representing scaled velocity. Upwelling is represented by positive values, and downwelling is represented by negative values. The dashed red circles represent the approximate location of the upstream pit and the downstream mound. The white areas indicate values near zero. The arrow illustrates the scale for velocities (cm/s).

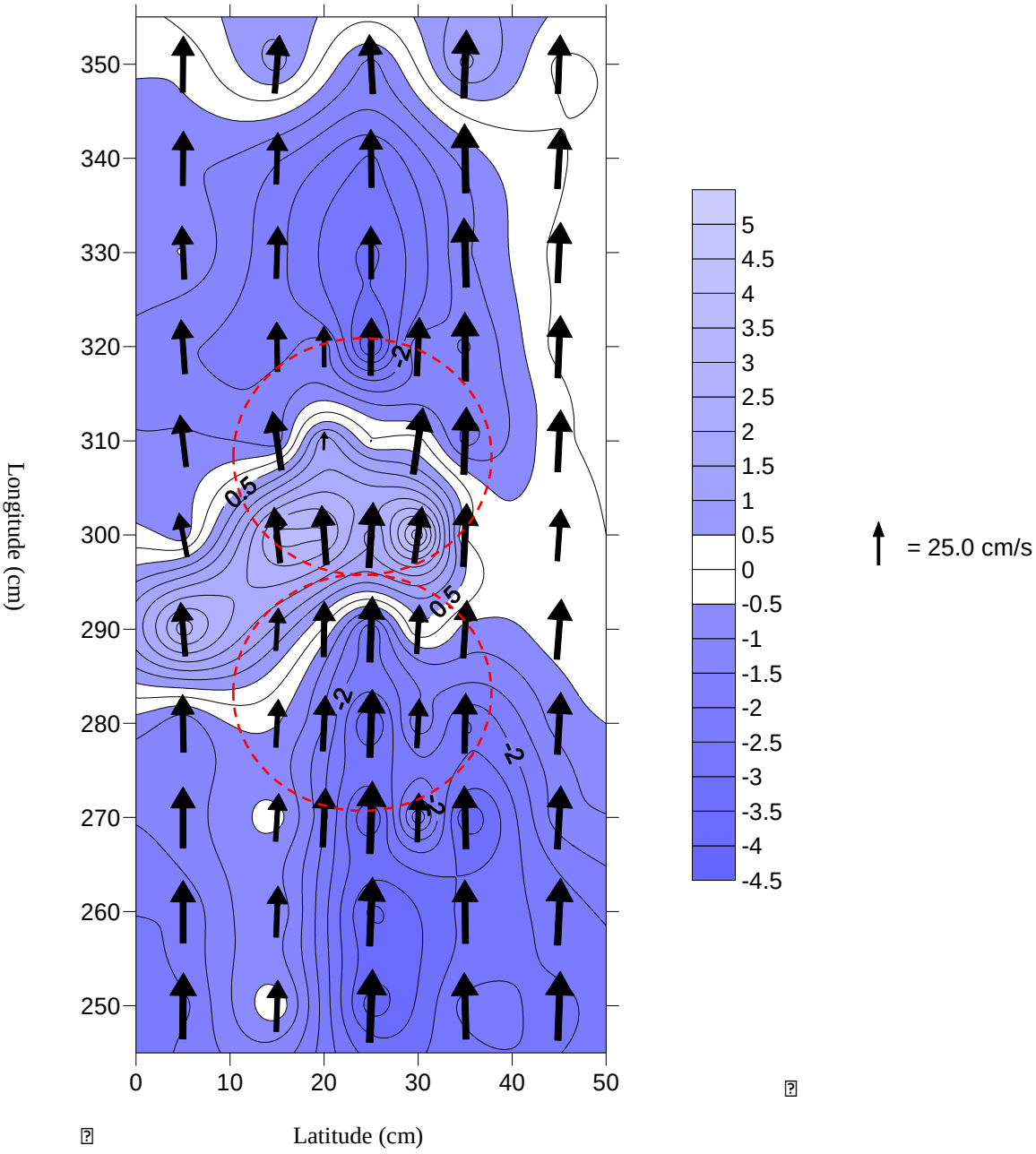

Figure 5.8. The average vertical velocity represented by isolines at a stage of 32.4 l/s with arrows representing scaled velocity. Upwelling is represented by positive values, and downwelling is represented by negative values. The dashed red circles represent the approximate location of the upstream pit and downstream mound. The white areas indicate values near zero. The arrow illustrates the scale for velocities (cm/s).

5.4. Turbulent Kinetic Energy

The TKE values were highest over the mound down the center of the redd at the 11.7 l/s flow rate. TKE was lowest immediately after the mound. The velocity correlates with the TKE values as the lowest velocity exists at the 310-cm longitudinal mark immediately downstream of the redd (Figure 5.9). The TKE values were highest over the mound down the center of the redd at the 19.5 l/s flow rate. TKE was lowest immediately after the mound at the 25-cm, 310-cm longitudinal mark. There is a slight increase at the 20-cm, 300-cm point and at the 35-cm, 300-cm point. The velocity again correlates with the TKE values as the lowest velocity exists at the 310 cm longitudinal mark immediately downstream of the redd (Figure 5.10). The TKE values were highest over the mound down the center of the redd at the 32.4 l/s flow rate. TKE was lowest immediately after the mound at the 25-cm, 310-cm point. There is a slight increase at the 20-cm, 290-cm point and at the 35-cm, 290-cm point. The velocity again correlates with the TKE values as the lowest velocity exists at the 310-cm longitudinal mark immediately downstream of the redd (Figure 5.11). However, this stage indicates areas of much larger TKE values at the mound and just downstream of the mound.

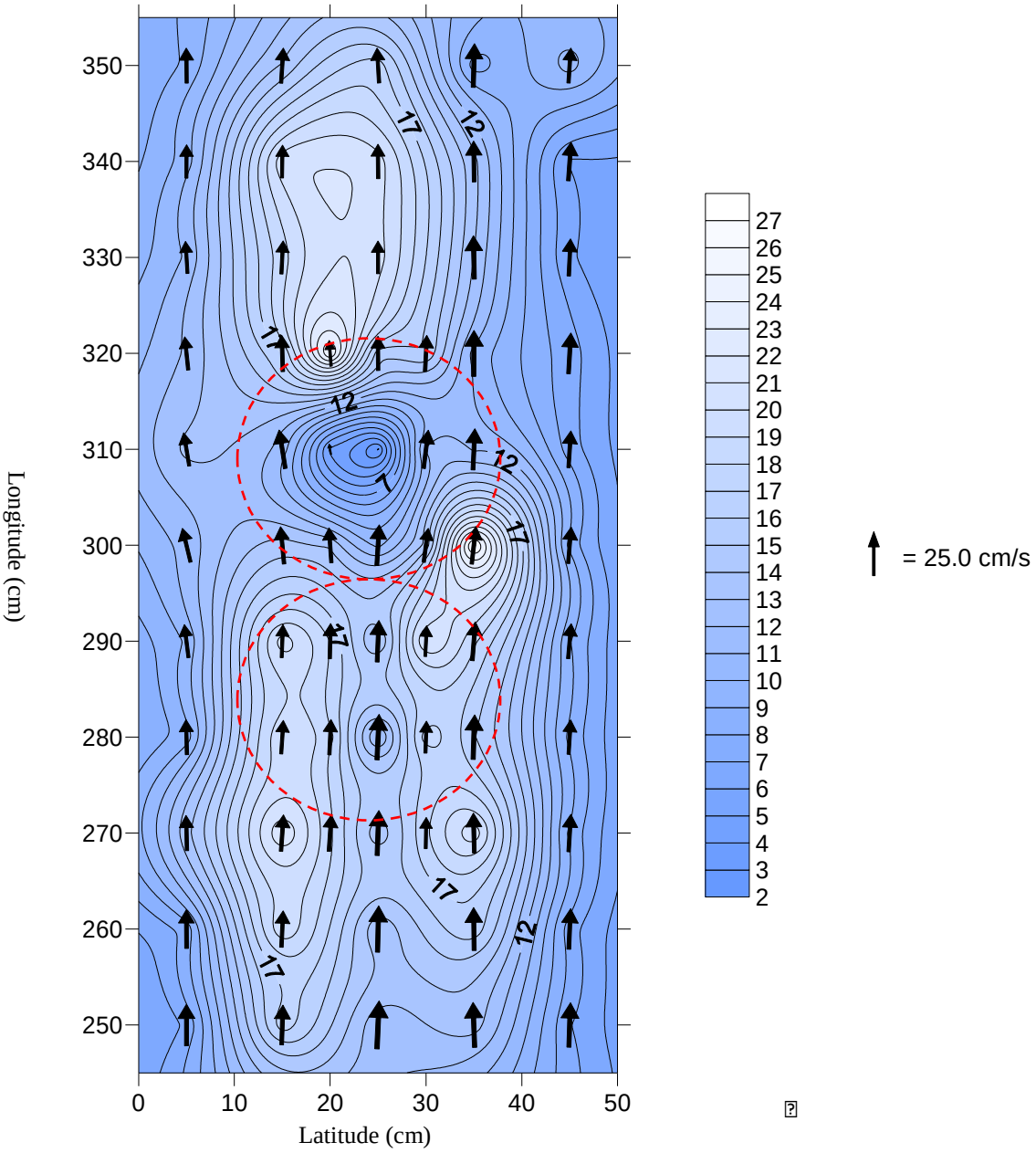

Figure 5.9. The average TKE (m^2/s^2) represented by isolines at a stage of 11.7 l/s with arrows representing scaled velocity. The dashed red circles represent the approximate location of the upstream pit and the downstream mound. The arrow illustrates the scale for velocities (cm/s).

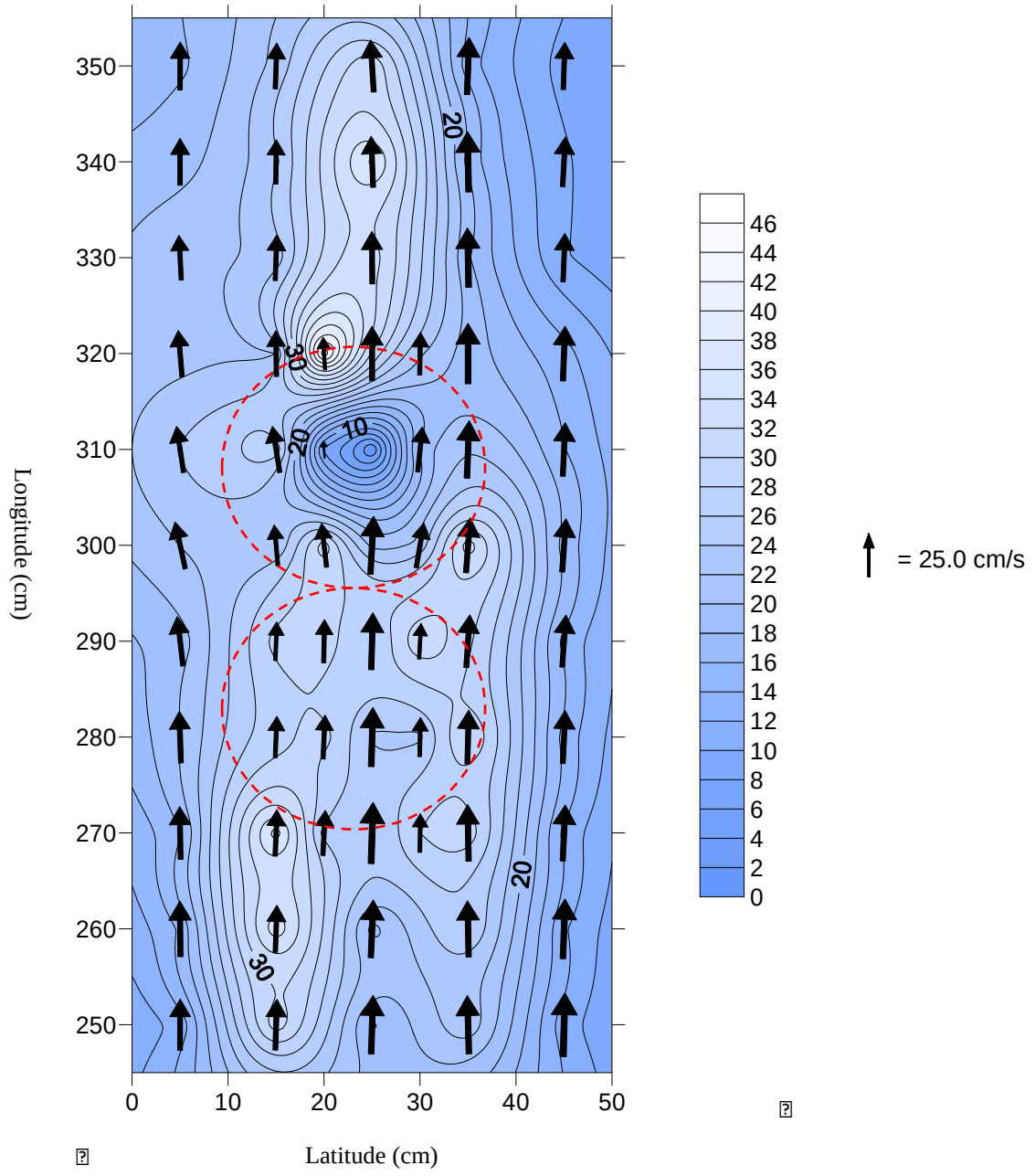

Figure 5.10. The average TKE (m^2/s^2) represented by isolines at a stage of 19.5 l/s with arrows representing scaled velocity. The dashed red circles represent the approximate location of the upstream pit and the downstream mound. The arrow illustrates the scale for velocities (cm/s).

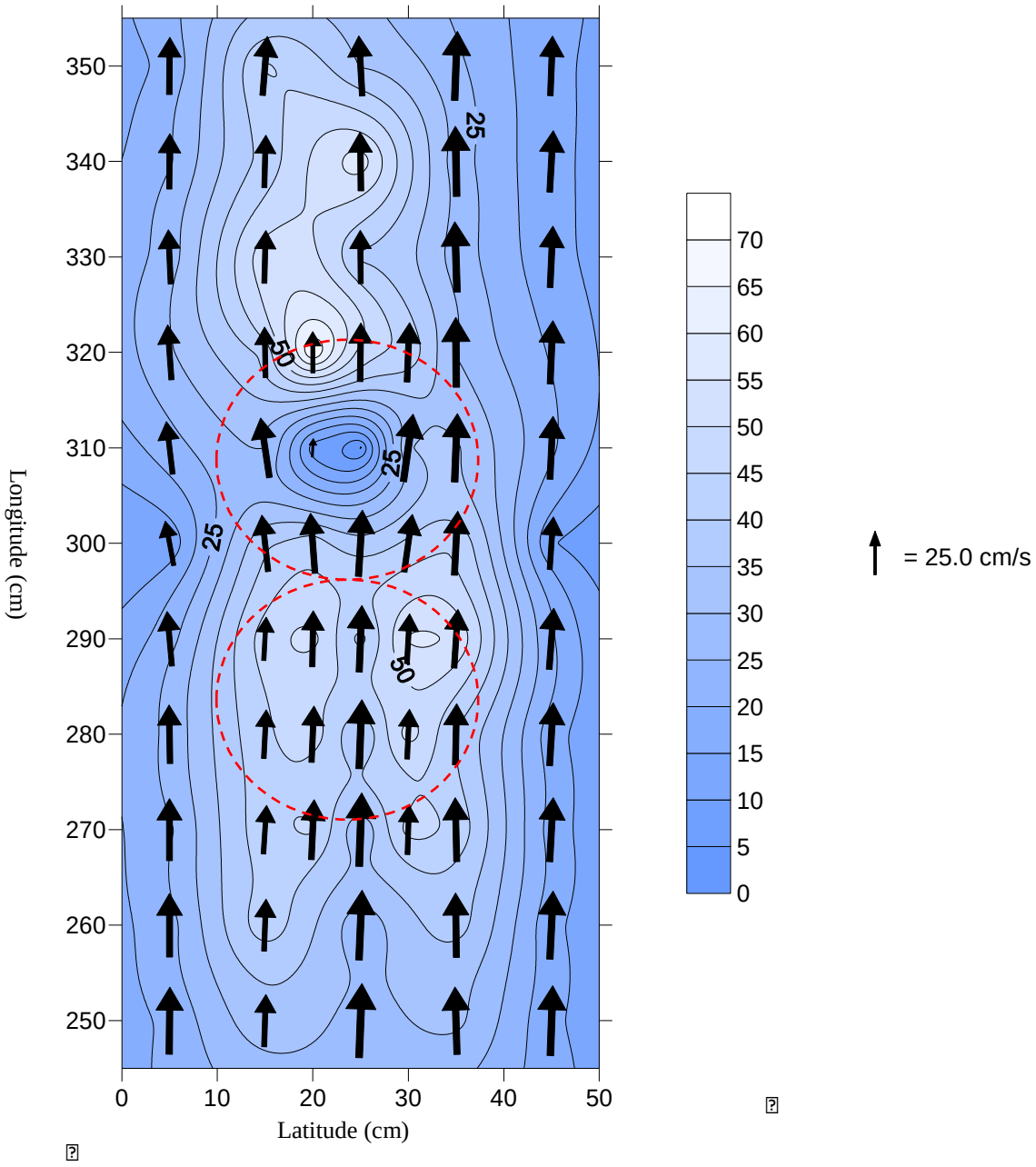

Figure 5.11. The average TKE (m^2/s^2) represented by isolines at a stage of 32.4 l/s with arrows representing scaled velocity. The dashed red circles represent the approximate location of the upstream pit and the downstream mound. The arrow illustrates the scale for velocities (cm/s).

5.5. Stage Variation of Turbulent Kinetic Energy

The increase in TKE is most notable between the 32.4 l/s and 19.5 l/s flow rates (Figure 5.13). The largest increases come before the mound at the 20-cm, 290-cm point and the 35-cm, 290-cm point. There is also an increase between the 20-cm and 320-cm to 330-cm points. There are slight increases in TKE between the 19.5 l/s and 11.7 l/s flow rates (Figure 5.12). The largest increases come before the mound at the 20-cm, 300-cm point and the 20-cm, 320-cm point.

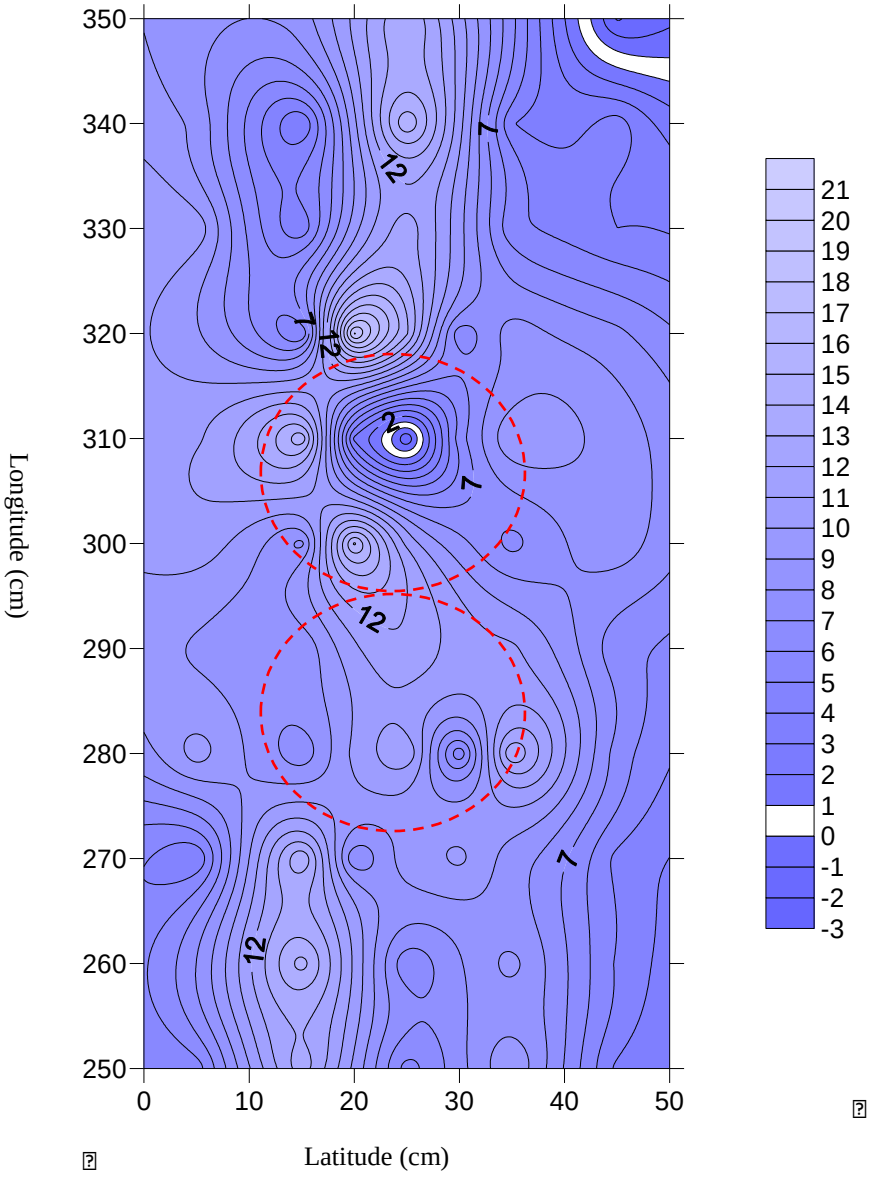

Figure 5.12. The difference in TKE m^2/s^2 represented by isolines between stages 19.5 l/s and 11.7 l/s. The dashed red circles represent the approximate location of the upstream pit and the downstream mound. The white areas indicate values near zero. The arrow illustrates the scale for velocities (cm/s).

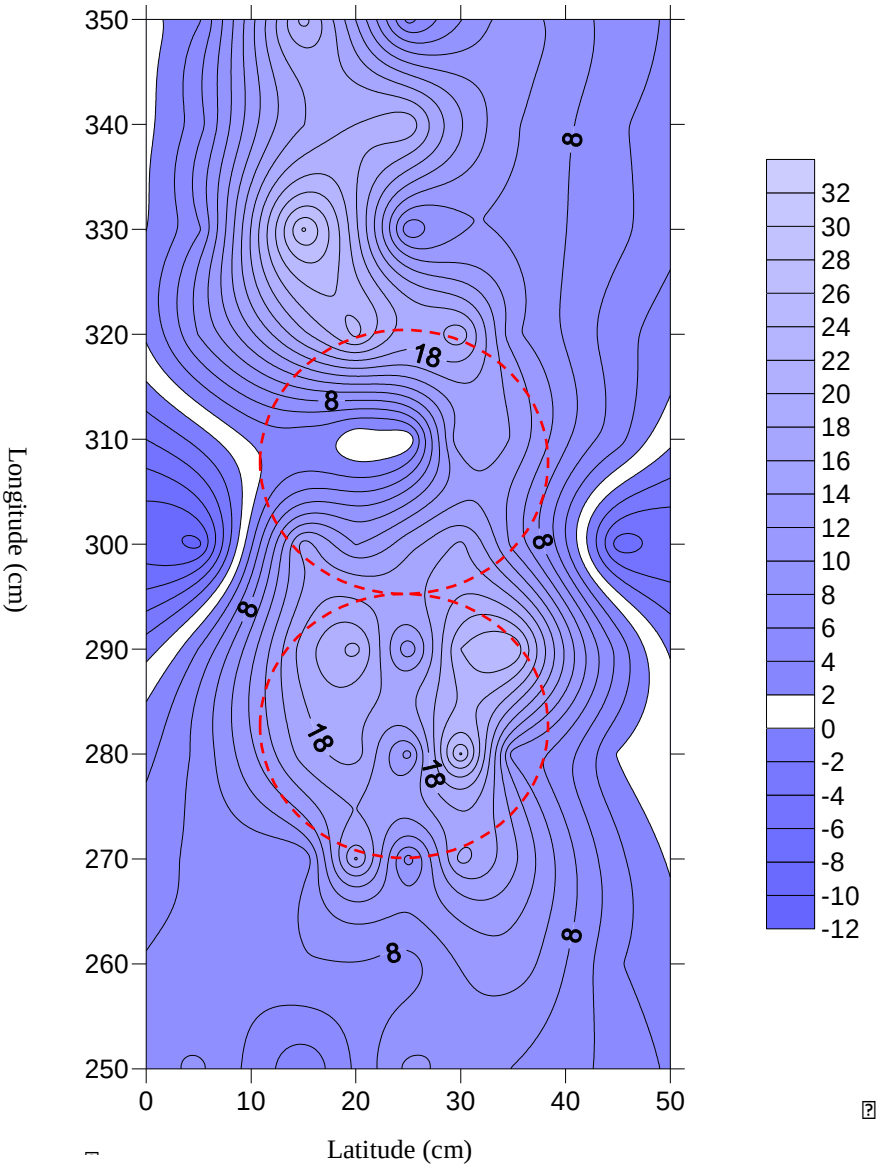

Figure 5.13. The difference in TKE m^2/s^2 represented by isolines between stages 32.4 l/s and 19.5 l/s. The dashed red circles represent the approximate location of the upstream pit and the downstream mound. The white areas indicate values near zero. The arrow illustrates the scale for velocities (cm/s).

5.6. Stage Variation of Mean Vertical Velocity

The mean vertical velocity increase is most apparent between the 32.4 l/s and 19.5 l/s flow rates. The largest increase was over the mound at the 20-cm, 300-cm point. The largest decrease was right before the mound at the 25-cm, 270-cm point, and moving up the mound at the 25-cm, 290-cm point (Figure 5.15). There are subtler differences in mean vertical velocity between the 19.5 l/s and 11.7 l/s flow rates. The largest increase was over the mound at the 35-cm, 300-cm point. The largest decrease was right after the mound at the 25-cm, 320-cm point (Figure 5.14).

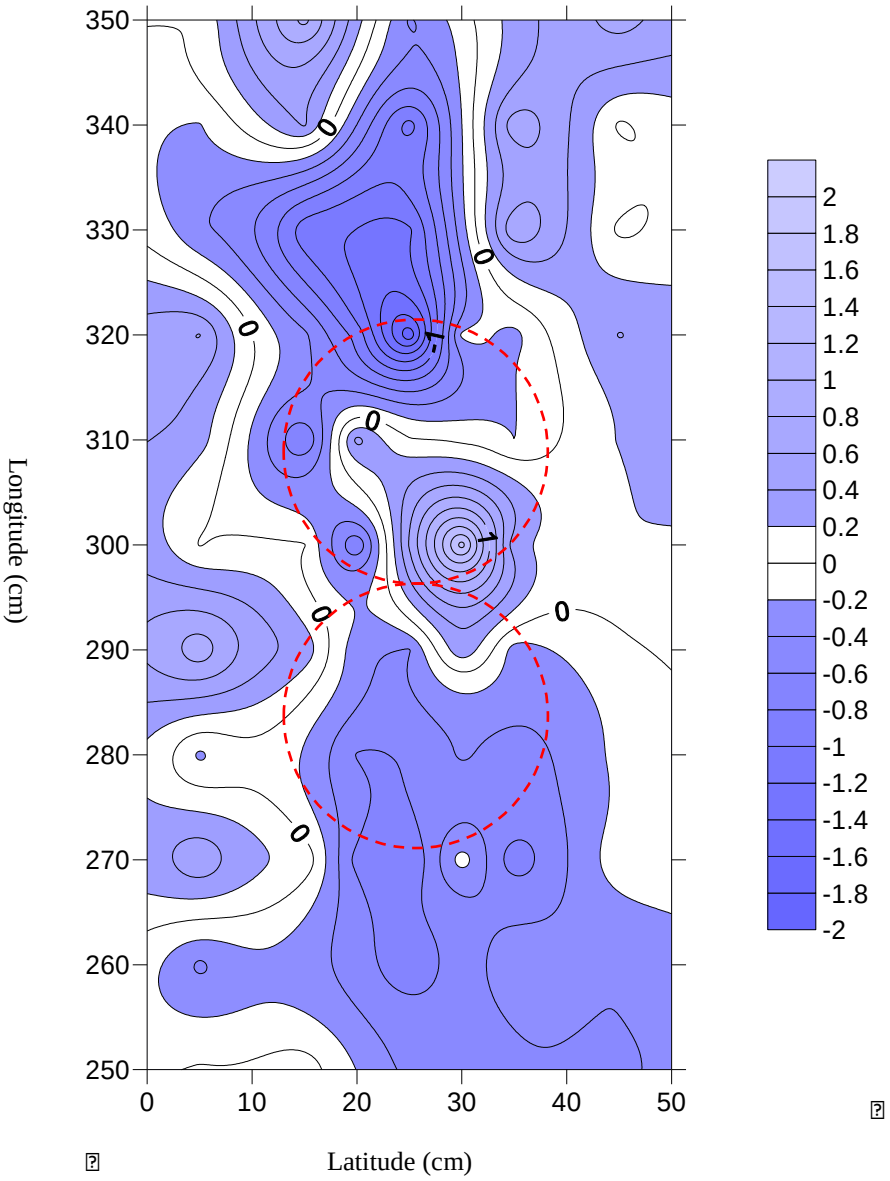

Figure 5.14. The difference in mean vertical velocity represented by isolines between stages 19.5 l/s and 11.7 l/s The dashed red circles represent the approximate location of the upstream pit and the downstream mound. The white areas indicate values near zero.

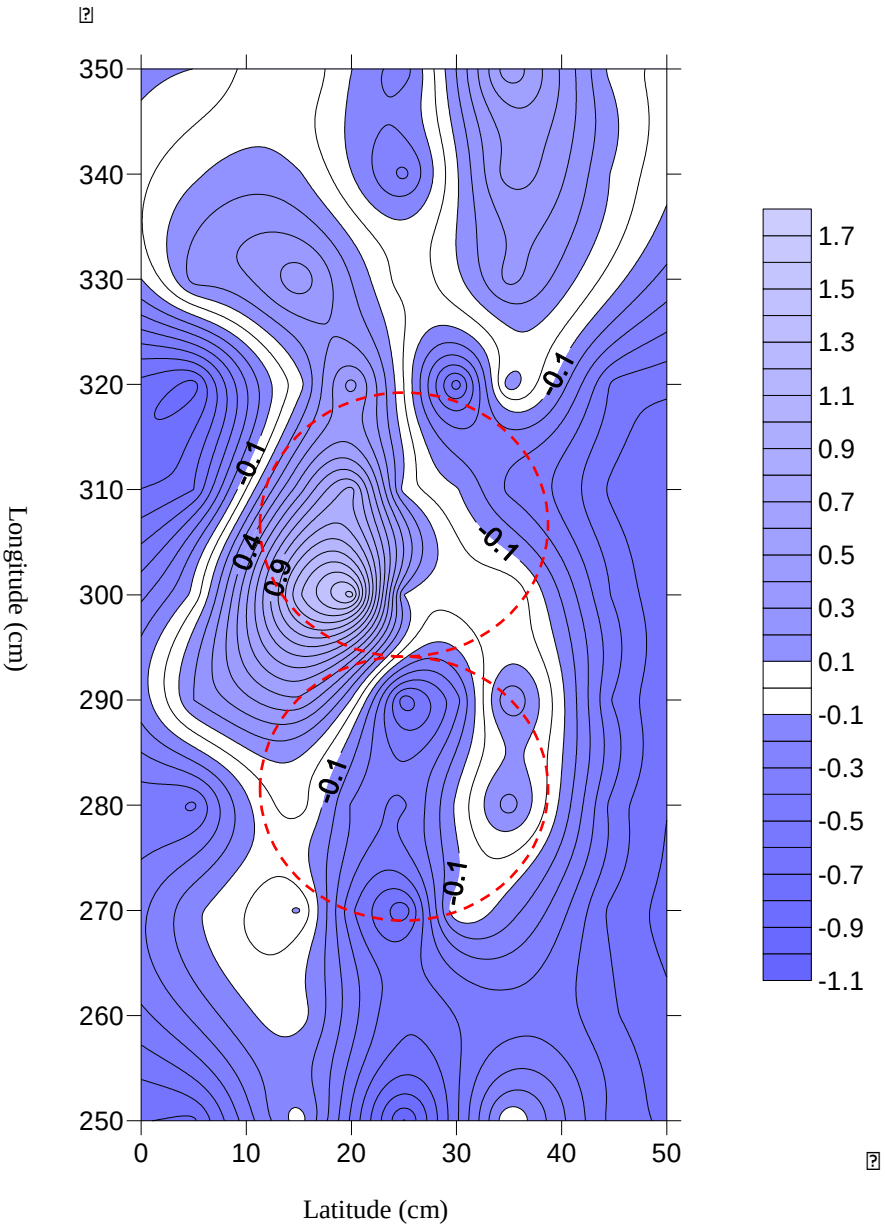

Figure 5.15. The difference in mean vertical velocity represented by isolines between stages 32.4 l/s and 19.5 l/s. The dashed red circles represent the approximate location of the pit and mound. The white areas indicate values near zero.

5.7. Salinity Injections

The salinity (ppm) for the first measured redd showed the larger rates of change at the 1.4-m, 1.3-m, 1.1-m, 1.0-m, 0.9-m, and 0.6-m marks running down the center of the redd (Figure 5.16). The 1.4-m, 1.1-m, mark injection sites were mid mound with the probe recording from downstream of the mound with a probe height of 4.5-cm and a distance of 0.39-cm and 0.69-m, respectively, from the injection sites. The 1.3-m injection site was slightly to the side of the mound with a probe height of 4.5-cm and a distance of 0.43-m from the injection site. This reading was the only one of five injections at the side of the center of the redd that showed variation in salinity levels. The 1.0-m, 0.9 m, and 0.6-m mark injection sites were all at the pit with the probe distance at the 1.25-m mark downstream (Figure 5.16). The probe heights for all these injections was 4.5-cm above the bed. All other injections had minor or no changes in salinity. The base of the pit showed the most variation in salinity for redd 2, and received the highest recording for the trials. The background salinity rate always returned to pre-injection levels after 30 seconds for all trials.

The salinity (ppm) for the second measured redd showed the greatest rates of change at the 0-m, 0.45-m, and 0.55 m marks running down the center of the redd (Figure 5.17). The 0.45-m and 0.55-m injections were over the pit with the probe height of 4.5-cm over the bed and 0.55-m and 0.45-m, respectively, downstream of the injection site. The 0 m injection site was at the base of the pit with a probe height of 4.5-cm over the bed and a distance of 0.3-m from the injection site. The base of the pit showed the most variation in salinity for redd 2, and received the highest recording for the trials. The background salinity was always returned to pre-injection levels after 30 seconds for all trials.

A concentrated dye solution was used in combination with the salinity injections to corroborate flow movement at the lamprey redd sites. Visual observation showed that the syringe injected some dye into the bed and some dye reappeared downstream. The dye that reappeared downstream took on average approximately 20 seconds to reappear 2 m downstream of the injection site. It then took about 10 seconds for the dye to disappear.

The results indicated that the topography of the redd greatly influences the movement of the flow by forcing multidirectional movement into the bed, laterally, or over the mound. The TKE values and vertical velocity values are highest at the mound. The downstream velocity was fastest down the center of the redd as the flow travelled down the pit, and downstream velocity slowed moving over the mound and was the slowest at the end of the mound. The salinity study showed the highest levels of response at the downstream end of the pit.

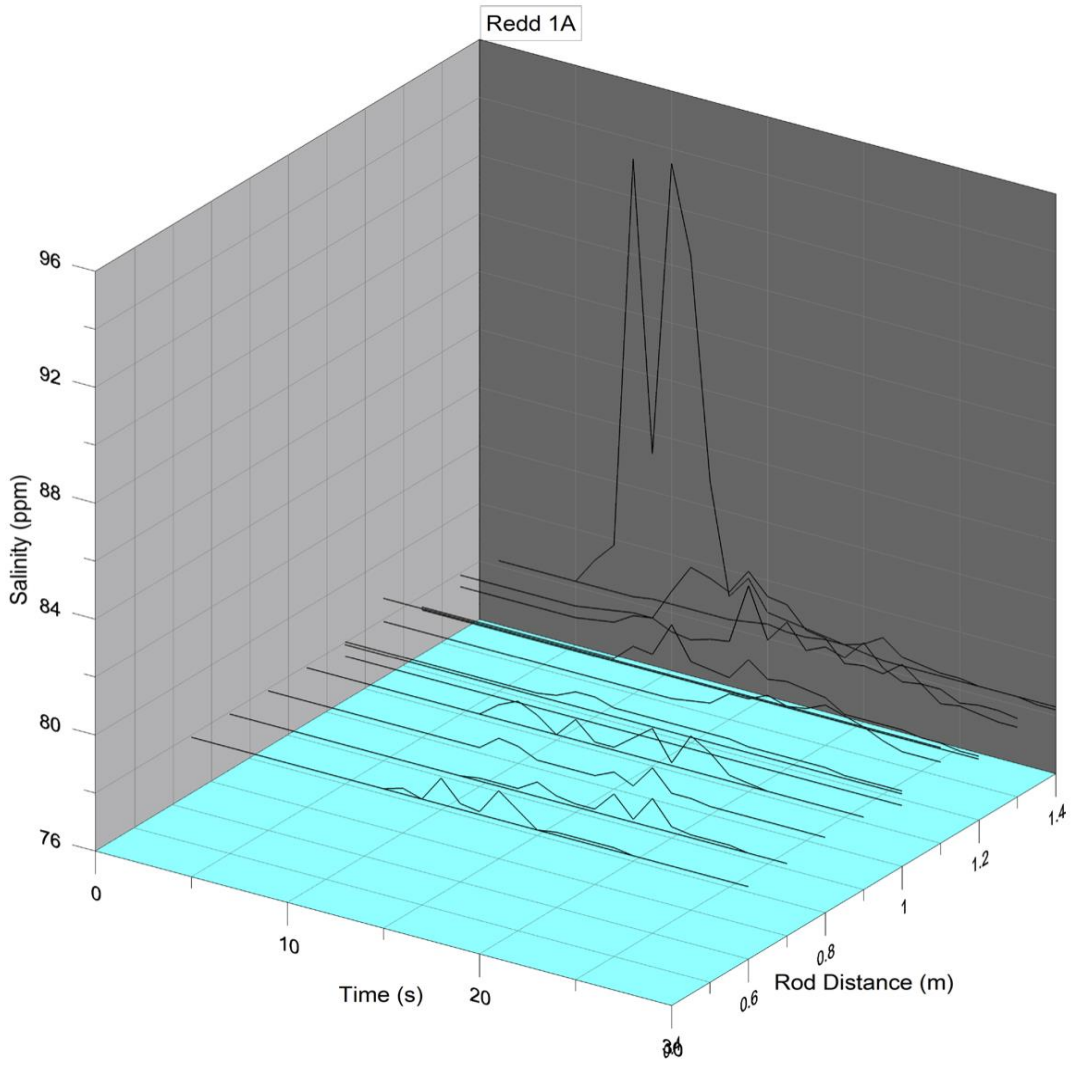

Figure 5.16. The salinity variation of redd 1 over time at different distances down the center line of the redd. The z-axis (Rod Distance) identifies a trial by spatial location. The y and x-axes represents the change in salinity over time, representing residence time. Each graph line represents one injection, with multiple trials at some sites. Some trials had no results.

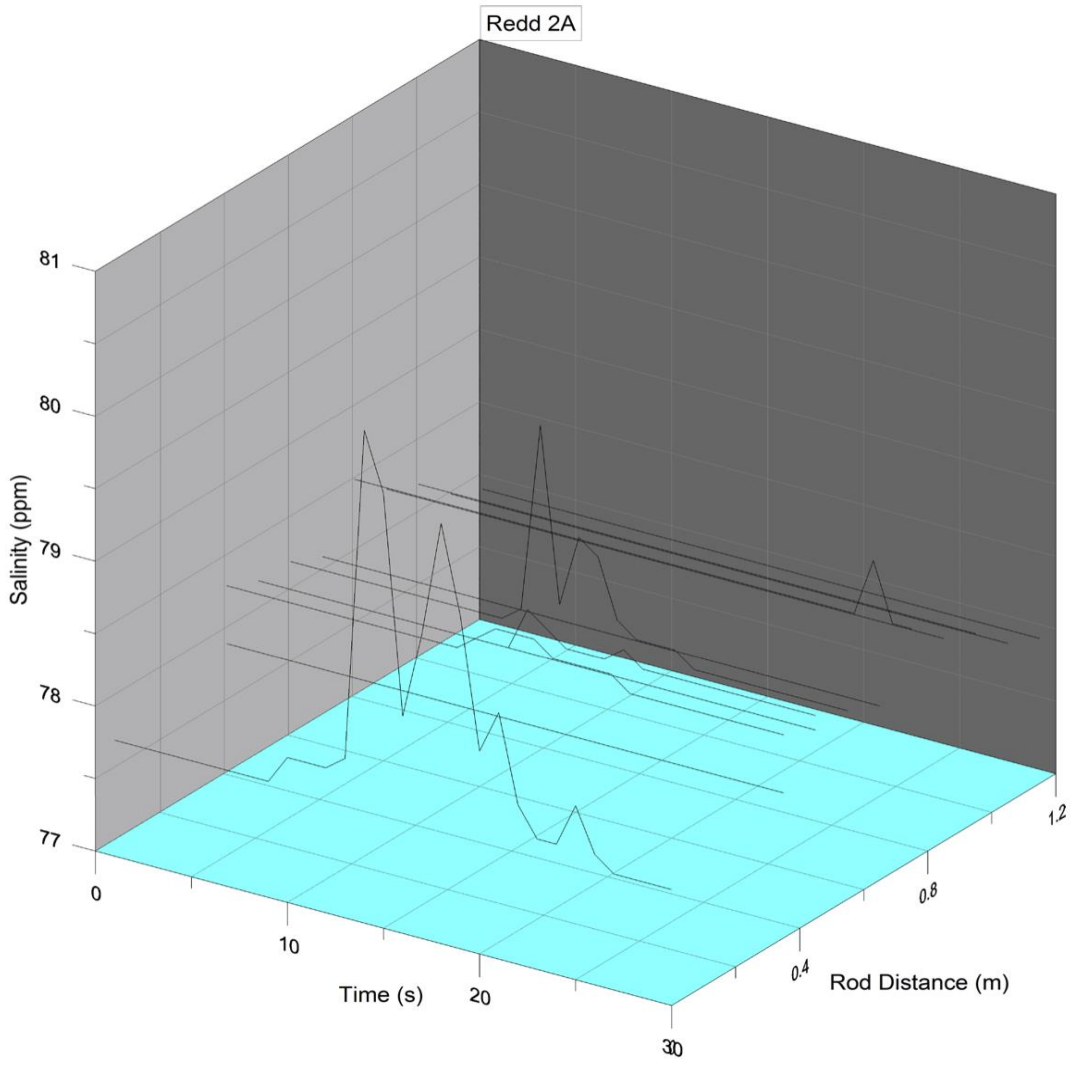

Figure 5.17. The salinity variation of redd 2 over time at different distances down the center line of the redd. The z-axis (Rod Distance) identifies a trial by spatial location. The y and x-axes represents the change in salinity over time, representing residence time. Each graph line represents one injection, with multiple trials at some sites. Some trials had no results.

6. Discussion

The combination of the field experiment and the flume experiment constructs a picture of how hyporheic flow operates within a redd. The flume experiment illustrates that the velocity and TKE patterns created by the redd cause areas of upwelling and downwelling moving over the redd. These patterns induce a low pressure zone just downstream of the mound, which suggests the presence of hyporheic flow in the redd. The field experiment demonstrates that when a salinity solution is injected into a redd there is some retention as water actually moves throughout the redd. The mechanisms behind the movement are represented by the flume study. The velocity of the hyporheic flow that moves through the redd is still unknown, but as a result of the salinity measurements, the movement is faster than 30 seconds per injection. It can be inferred that the higher the flow rate, the stronger the differences of low and high pressure zones existing at the redd, thereby causing faster hyporheic velocities.

The results of the flume study indicate strong areas of downwelling and upwelling at the pit and mound, respectively, with increases in higher stage. These results are shown by the vertical mean velocity outcomes and the TKE values. This data suggests that moving downstream over the redd, especially down the center of the redd (which contains the highest and lowest topographical heights) that the flow increases and decreases in velocity creating areas of downwelling and upwelling. The high levels of turbulence after the mound at all stages indicates that the mound forces the creation of an eddy downstream of the mound, therefore slowing down velocity immediately after the mound because of vortex shedding. The presence of the eddy could also be an indication of some upstream movement lower to the bed than was measured. The presence of the eddy signifies good fluid mixing downstream of the mound. The Vz values all increase after the mound and increase with higher stage, similar to the TKE values.

The increase in TKE values as stage increases creates a stronger eddy system downstream of the mound. The resulting turbulence from the eddy at the higher stages would cause more mixing.

The Vz values show upwelling at the mound. This illustrates the pit and mound force the flow upwards, which reduces the velocity downstream of the mound. The water surface slope of the Blackledge River suggests higher pressure upstream of the mound, similar to the water surface slope in the flume. The rapid decrease of velocity downstream of the mound could be an indication of hyporheic flow moving through the redd because the low velocity values suggest a low pressure zone downstream of the mound. This low pressure zone would cause an induction of flow through the cobbles of the mound. The increase in Vz values as stage increases suggests that during spawning times at the higher discharges the hyporheic exchange is more vital. This phenomenon is most obvious at the medium and high flow stages of 19.5 l/s and 32.4 l/s. These flow rates are most likely when a lamprey would spawn in a riverine environment, and the conditions created by the redd and higher flows would improve hyporheic exchange into the mound when the eggs require vital dissolved oxygen and nutrients. The flow movement through the redd might also aid in getting the spawning eggs into the mound.

The results of the salinity syringe injection method appear to support the suggestion of the induced hyporheic exchange at the redd. The injection sites just before the mound for redd 1 and redd 2 indicated the highest retention rates of salinity with all other injections showing minor or no change. These injections indicated good variability and retention of salinity compared to injections further upstream of the mound. The results indicate the strongest areas of downwelling, percent change, and variability when injected in the pit just upstream of the mound. These areas of injection tended to contain a good mix of cobbles and gravels that caused a faster rate of flow through the mound.

The areas where the salinity probe did not pick up any readings might suggest the salinity solution might be going into the bed and traveling through the sediment and underneath the probe. The reason for this phenomenon might be a result of groundwater flow underneath the hyporheic zone. The concentrated dye solution confirms this theory because the visual observations showed that the syringe injected some dye at the downstream end of the pit and some dye reappeared farther downstream. This can be translated to the salinity injection method because both tended to have slow decay rates. Low hydraulic conductivity might be a reason why some salinity readings had low values. Difficulty in inserting the injection probe into the bed suggests tightly compacted sediments. The compact substrate might limit the downstream movement of the saline solution. The field experiment, while difficult to directly measure hyporheic velocity, showed that there is certainly instances of hyporheic exchange within lamprey redds, especially just before and into the mound.

Hyporheic flow processes within spawning redds is important for the egg survival rates. Redd construction results in increased hydraulic conductivity because of sediment sorting and forced downwelling and upwelling (Bowerman et al., 2014). Understanding the processes at lamprey redds is crucial for the continued conservation of lamprey. The saline injection results are impactful because the data showed that there appeared to be low hydraulic conductivity at redd 1 and redd 2, which both showed minimized salinity readings farther upstream from the mound. Both redds showed similar trends in readings, which suggests that they are constructed relatively similarly. The low hydraulic conductivity is probably a result of the intrusion of fines in the redd structures. The presence of fines in the redds found in the field might suggest that the redds were not new features. However, the hydraulic conductivity in the flume experiment appeared to be greater because of relative lack of fines in the redd structure. The flume

experiment and the field experiment showed similar results in relation to the upstream end of the mound causing the highest upwelling and peak salinity readings.

The results of the field study agree with the scientific literature in that most studies indicate that quantifying hyporheic flow is difficult. Packman et al., 2004 notes that the relationships between hyporheic exchange and bed-form scale with the square of the stream Reynolds number, but understanding of this process is still ongoing. The flume study does not relate to any present literature because this methodology has not been used to examine hyporheic flow at a scaled lamprey redd.

The flume experiment appears to represent a reliable dataset because of the methodology and the equipment used. The computational analysis was robust and the topographic maps illustrate what is happening within the lamprey redds. However, the saline injection experiment data might not be as reliable because it is impossible to construct an accurate picture of the movement of the flow, and the dye tracer might not accurately represent the movement of the flow because of the flow around the probe. The assumptions that were made about the injections are not as reliable as the assumptions made in the flume. Future research might include a combination of a saline solution and dye solution that would illustrate what is happening in real time. The flume experiment might involve a dye tracer experiment as well, so multiple tests can be repeated. This study could be repeated on salmon redds because of their similar structure to lamprey redds.

7. Conclusion

The flume and field experiments provided strong evidence for the operation and presence of hyporheic flow within lamprey redds. The upwelling and downwelling flows and their increases at higher stage indicate how the topography stimulates variations in flow and causes vertical movement. The velocity created by the redd in combination with the TKE and Vz values illustrates the existence of a low pressure zone just downstream of the mound. This low pressure zone suggests that the high pressure zones with faster velocities upstream of the mound might be drawn through the mound by the low pressure zone. The addition of the field experiment is useful in adding supplementary knowledge on the retention and movement of water through the redd. The experiment indicates that there is water moving through the redd, especially just before the mound, although the direction and exact velocity is unknown.

The presence of hyporheic flow within lamprey redds is important for the understanding of exactly why redds are created. The hyporheic flow causes the exchange of DO and nutrients essential for the eggs and juvenile lamprey in the mound. The processes of hyporheic flow within redds is still largely unknown, but this study provides strong evidence that it does operate within lamprey redds and increases with higher stage. Future research needs to expand on the salinity and tracer method. The data would be strengthened if a 3-D hyporheic model was used with the redd topography. This thesis study provides a good start to a process that remains complicated, especially within lamprey redds.

8. References

Benjankar, R., Tonina, D., Marzadri, A., McKean, J., & Isaak, D. J., 2016. Effects of habitat quality and ambient hyporheic flows on salmon spawning site selection. *Journal of Geophysical Research: Biogeosciences*, *121*(5), 1222-1235.

Boulton, A. J., Findlay, S., Marmonier, P., Stanley, E. H., & Valett, H. M., 1998. The Functional Significance of the Hyporheic Zone in Streams and Rivers. A*nnual Review of Ecology and Systematics*, 29(1), 59-81.

Bowerman, T., Neilson, B. T., & Budy, P., 2014. Effects of fine sediment, hyporheic flow, and spawning site characteristics on survival and development of bull trout embryos. *Canadian Journal of Fisheries and Aquatic Sciences*, *71*(7), 1059-1071.

Brunke, M., 1999. Colmation and depth filtration within streambeds: retention of particles in hyporheic interstices. *International Review of Hydrobiology*, *84*(2), 99-117.

Brunke, M., & Gonser, T., 1997. The Ecological Significance of Exchange Processes Between Rivers and Groundwater. *Freshwater Biology*, 37(1), 1-33.

Brandt, S. A., 2000. Classification of geomorphological effects downstream of dams. *Catena*, 40(4), 375-401.

Buffington, J. M., & Tonina, D., 2009. Hyporheic exchange in mountain rivers II: effects of channel morphology on mechanics, scales, and rates of exchange. *Geography Compass*, 3(3), 1038-1062.

Cardenas, M. B., Wilson, J. L., & Zlotnik, V. A., 2004. Impact of heterogeneity, bed forms, and stream curvature on subchannel hyporheic exchange. *Water Resources Research*, *40*(8).

Castro, N. M., & Hornberger, G. M., 1991. Surface-subsurface water interactions in an alluviated mountain stream channel. *Water Resources. Res, 27*(7), 1613-1621.

Findlay, S., 1995. Importance of Surface-Subsurface Exchange in Stream Ecosystems: The Hyporheic Zone. *Limnology and Oceanography*, 40(1), 159-164.

Fremier, A. K., Seo, J. I., & Nakamura, F., 2010. Watershed controls on the export of large wood from stream corridors. *Geomorphology, 117*(1), 33-43.

Fuller, P., L. Nico, E. Maynard, J. Larson, A. Fusaro, & A.K. Bogdanoff. 2016. Petromyzon marinus. *USGS Nonindigenous Aquatic Species Database,* Gainesville, FL.

Harvey, J. W., & Bencala, K. E., 1993. The effect of streambed topography on surface subsurface water exchange in mountain catchments. *Water Resources Research, 29*(1), 89-98.

Harvey, J. W., Wagner, B. J., & Bencala, K. E., 1996. Evaluating the Reliability of the Stream Tracer Approach to Characterize Stream-Subsurface Water Exchange. *Water Resources Research Water*, 32(8), 2441-2451.

Kasahara, T., & Wondzell, S. M., 2003. Geomorphic controls on hyporheic exchange flow in mountain streams. *Water Resources Research, 39*(1).

Montgomery, D. R., J. M. Buffington, R. D. Smith, K. M. Schmidt, & G. Pess, 1995. Pool Spacing in Forest Channels, *Water Resources. Res*., 31(4), 1097–1105.

NOAA Fisheries., 2015. Atlantic salmon (Salmo salar).

Packman, A. I., Salehin, M., & Zaramella, M., 2004. Hyporheic exchange with gravel beds: basic hydrodynamic interactions and bedform-induced advective flows. *Journal of Hydraulic Engineering, 130*(7), 647-656.

Storey, R. G., Howard, K. W., & Williams, D. D., 2003. Factors Controlling Riffle-Scale Hyporheic Exchange Flows and Their Seasonal Changes in a Gaining Stream: A Three Dimensional Groundwater Flow Model. *Water Resources Research*, 39(2).

Thompson, D. M., 2006. The role of vortex shedding in the scour of pools. *Advances in Water Resources*, *29*(2), 121-129.

Trauth, N., Schmidt, C., Maier, U., Vieweg, M., & Fleckenstein, J. H., 2013. Coupled 3-D Stream Flow and Hyporheic Flow Model Under Varying Stream and Ambient Groundwater Flow Conditions in a Pool-riffle System. *Water Resources Research*, 49(9), 5834-5850.

Veličković, B., 2005. Colmation as one of the processes in interaction between the groundwater and surface water. *Facta universitatis-series: Architecture and Civil Engineering*, *3*(2), 165-172

Appendix A: Raw Field Data

All lamprey redd GPS coordinates

N41 37.028 W72 25.575	
N41 37.049 W72 25.587	
N41 40.774 W72 27.709	
N41 40.733 W72 27.658	
N41 40.690 W72 27.667	
N41 40.663 W72 27.672	
N41 40.632 W72 27.678	
N41 40.625 W72 27.674	
N41 34.933 W72 25.356	
N41 34.949 W72 25.347	
N41 35.278 W72 25.218	
N41 35.284 W72 25.211	
N41 35.352 W72 25.173	
N41 35.354 W72 25.169	
N41 36.479 W72 25.575	Sampled
N41 36.480 W72 25.576	Sampled
N41 36.488 W72 25.568	Sampled
N41 36.507 W72 25.562	Sampled
N41 36.505 W72 25.564	Sampled
N41 36.502 W72 25.576	Sampled
N41 36.500 W72 25.570	Sampled
N41 36.500 W72 25.565	Sampled
one additional redd her	Sampled

Lamprey redd phi size classification

Site			Sample A	Redd Upper UPS Pit
	Total Mas	2916.4		
Phi Size	Sieve Siz	Class Mas	Class Per	Percent Finer
-8	256 mm	0	0	100
-7.5	181 mm	0	0	100
-7	128 mm	0	0	100
-6.5	91 mm	0	0	100
-6	64 mm	0	0	100
-5.5	45 mm	200	0.06858	93.14223015
-5	32 mm	300	0.10287	82.85557537
-4.5	23 mm	419.4	0.14381	68.47483198
-4	16 mm	541.8	0.18578	49.89713345
-3.5	11 mm	545.2	0.18694	31.20285283
-3	8.0 mm	232.9	0.07986	23.21697984
-2.5	5.7 mm	157.4	0.05397	17.81991496
-2	4.0 mm	87.1	0.02987	14.83335619
-1.5	2.8 mm	78.9	0.02705	12.12796599
-1	2.0 mm	68	0.02332	9.796324235
-0.5	1.4 mm	63.2	0.02167	7.629268962
0	1.0 mm	65.5	0.02246	5.383349335
0.5	0.71 mm	58.9	0.0202	3.363736113
1	0.50 mm	52.8	0.0181	1.553284872
1.5	Pan	45.3	0.01553	3.55271E-15
	Total Mas	2916.4	1	

Site			Sample A	Large Redd Mound
	Total Mas	32762.1		
Phi Size	Sieve Siz	Class Mas	Class Per	Percent Finer
-8	256 mm	0	0	100
-7.5	181 mm	0	0	100
-7	128 mm	0	0	100
-6.5	91 mm	2480	0.0757	92.43027767
-6	64 mm	17820	0.54392	38.03815995
-5.5	45 mm	10520	0.3211	5.927886186
-5	32 mm	1740	0.05311	0.616871324
-4.5	23 mm	200	0.0061	0.006409846
-4	16 mm	0	0	0.006409846
-3.5	11 mm	0	0	0.006409846
-3	8.0 mm	0	0	0.006409846
-2.5	5.7 mm	0	0	0.006409846
-2	4.0 mm	0.5	1.5E-05	0.004883692
-1.5	2.8 mm	0.5	1.5E-05	0.003357538
-1	2.0 mm	0.4	1.2E-05	0.002136615
-0.5	1.4 mm	0.3	9.2E-06	0.001220923
0	1.0 mm	0.2	6.1E-06	0.000610461
0.5	0.71 mm	0.1	3.1E-06	0.000305231
1	0.50 mm	0.1	3.1E-06	4.92748E-15
1.5	Pan	0	0	4.92748E-15
	Total Mas	32762.1	1	

Site			Sample ?	Large Redd Pitt
	Total Mas	5253.86		
Phi Size	Sieve Siz	Class Mas	Class Per	Percent Finer
-8	256 mm	0	0	100
-7.5	181 mm	0	0	100
-7	128 mm	0	0	100
-6.5	91 mm	3.56	0.00068	99.9322403
-6	64 mm	0	0	99.9322403
-5.5	45 mm	0	0	99.9322403
-5	32 mm	265	0.05044	94.88832972
-4.5	23 mm	698.2	0.13289	81.59905289
-4	16 mm	1295.5	0.24658	56.94099196
-3.5	11 mm	887.7	0.16896	40.04484322
-3	8.0 mm	519.9	0.09896	30.14926169
-2.5	5.7 mm	375.9	0.07155	22.99452212
-2	4.0 mm	192.5	0.03664	19.33054935
-1.5	2.8 mm	171.7	0.03268	16.06247597
-1	2.0 mm	154.8	0.02946	13.11607085
-0.5	1.4 mm	165.9	0.03158	9.958392496
0	1.0 mm	176.6	0.03361	6.597054356
0.5	0.71 mm	146.2	0.02783	3.81433841
1	0.50 mm	110.6	0.02105	1.709219507
1.5	Pan	89.8	0.01709	2.88658E-15
	Total Mas	5253.86	1	

Appendix B: Calculations and Statistical Results

Connecticut College flume hertz numbers converted from the scaled Froude numbers from the discharges from the USGS database for the month of June at Station 01193500.

Hz	Depth	Discharge		Depth of water (m)	Discharge m^3/s	Velocity (m/s)	Fr
40	141.87	25.01	0.14187	0.08946	0.02501	0.559132573	0.596952821
45	152.51	28	0.15251	0.1001	0.028	0.559440559	0.564646412
50	156.6	31.4	0.1566	0.10419	0.0314	0.602744985	0.596293738
53	159.53	33.9	0.15953	0.10712	0.0339	0.632935026	0.617537749
56	161.78	35.6	0.16178	0.10937	0.0356	0.651001189	0.628597049
60	162.59	37.8	0.16259	0.11018	0.0378	0.686149936	0.660096311
62.5	163.49	39.1	0.16349	0.11108	0.0391	0.703997119	0.674516548
24.5	157.44	11.7	0.15744	0.10503	0.0117	0.222793488	0.219525751
33.5	167.81	19.5	0.16781	0.12475	0.0195	0.312625251	0.282646387

Peak discharge from USGS station 01193500 converted to flume l/s, which was then used to scale the flume discharge stages.

	date	ft^s	flume l/s
peak	6-Jun	166	32.4
	11:am at 6/9	100	19.5
	12 pm at 6/9	60	11.7

Significant difference chart for depth at Mound vs. Pit at the surveyed lamprey redds.

Depth		
Sections compared	Mean Difference	Significant
UPS 1 – UPS 2	-0.0138	No
DS 1 – DS 2	0.03092	No
DS 1 – UPS 1	-0.0555	Yes
DS 1 – UPS 2	-0.0417	Yes
DS 2 – UPS 1	-0.0246	No
DS 2 – UPS 2	-0.0108	No
Pit - Mound	**-0.2239**	**Yes**
Pit – UPS 1	0.21475	Yes
Pit – UPS 2	0.08475	Yes
Pit – DS 1	-0.1264	Yes
Pit – DS 2	-0.0955	Yes
Mound – UPS 1	-0.153	Yes
Mound – UPS 2	-0.1392	Yes
Mound – DS 1	0.0975	Yes
Mound – DS 2	0.12842	Yes

Significant difference chart for the Froude number values at the Pit vs. Mound at the surveyed lamprey sites.

Froude Numbers		
Sections compared	Mean Difference	Significant
UPS 1 – UPS 2	-0.006	No
DS 1 – DS 2	-0.0161	No
DS 1 – UPS 1	0.1152	No
DS 1 – UPS 2	0.12117	No
DS 2 – UPS 1	0.09913	No
DS 2 – UPS 2	0.10509	No
Pit - Mound	**0.61447**	**Yes**
Pit – UPS 1	-0.179	Yes
Pit – UPS 2	-0.1731	Yes
Pit – DS 1	0.29422	Yes
Pit – DS 2	0.27815	Yes
Mound – UPS 1	0.43544	Yes
Mound – UPS 2	0.44141	Yes
Mound – DS 1	-0.3202	Yes
Mound – DS 2	-0.3363	Yes

Appendix C: Additional Graphs

Graph showing the topographical profile variation of every lamprey redd with the value 0 being the center of the pit.

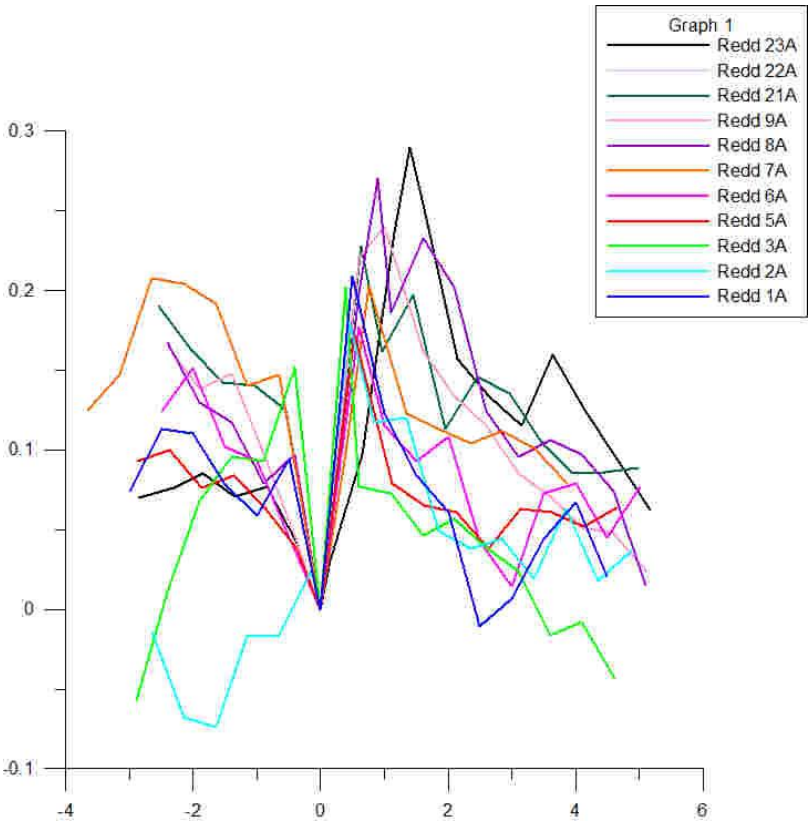

Graph showing the phi size variation for the pit vs. mound for all surveyed lamprey redds.